الجمهورية الجزائرية الديمقراطية الشعبية
People's Democratic Republic of Algeria
Ministry of Higher Education And Scientific Research
University Abdelhamid Ibn Badis Mostaganem
وزارة التعليم العالي و البحث العلمي
جامعة عبد الحميد بن باديس مستغانم

Department of Process Engineering
قسم هندسة الطرائق

Ref :……../U.M/F.S.T/2025
رقم: ..... / ج .م/ ك.ع.ت//2025

ACADEMIC MASTER'S DISSERTATION

Sector: PROCESS ENGINEERING

Specialty: ENVIRONMENTAL PROCESS ENGINEERING

THEME

Degradation of Anthraquinone Dye AG-25 Using CNF400 Nanoferrite via a Dark Heterogeneous Fenton Process

Presented by

1- BOUMAZA Somia
2- CHAIB Chahinez

Defended on 03/06/ 2025 before the jury composed of:

President:	DRIOUCH Aouatef	Professor	UMAB
Examiner:	SLAMANI Samira	Assistant Professor B	UMAB
Supervisor:	ABDELMALEK Fatiha	Professor	UMAB
Co-Supervisor:	BENDAHMAN Rachida	PhD Student	UMAB

Academic year 2024 / 2025

Dedication

With deep gratitude and all our love, we dedicate this work to the two most precious sources of support in our lives.

To our families. To our parents, who have made countless sacrifices and offered us unwavering confidence and unconditional support throughout this academic journey. To our mothers and fathers, and to our beloved brothers and sisters. Your patience, love, and encouragement carried us through every obstacle. Every night of studying, every challenge overcome, every achievement attained was also made possible thanks to your constant presence and belief in us

To Meriem and Farhanez, for their loyal friendship, attentive presence, and constant support.

Acknowledgements

We would like to first and foremost thank Almighty God for giving us the health, strength and patience to bring this final year to a successful completion.

We would like to also extend our greatest thanks to our supervisor, professor **Fatiha ABDELMALEK**, Director of the **STEVA** laboratory, for trusting us, for the time she dedicated, for her moral support and for the pertinent advice we were given throughout this work.

We would like to express our sincere thanks and deep respect to professor **A. ADDOU** for his constant availability, and for the helping hand and support he allotted to us.

We extend our heartfelt thanks to our co-supervisor, **Rachida BENDAHMAN**, for her constant encouragement and valuable guidance. Her support in supervising this research and assisting with the writing process enabled us to make significant and meaningful progress.

We warmly thank all the members of the jury, particularly the president, Mrs **Aouatef DRIOUCH**, and the examiner, Mrs **Samira SLAMANI**, for the honor of evaluating our work.

We would also take this opportunity to thank the whole STEVA laboratory team and all its members for the encouragement and support we received throughout this project.

Finally, we would sincerely like to thank everyone who contributed, be it directly or indirectly, to the realization of this work.

List of figures

List of tables

List of abbreviations

UMAB	University Abdelhamid Ibn Badis – Mostaganem
ABS	Absorbance
AG25	Acid green 25
AOP	Advanced oxidation process
AS	Actives sites
AQ	Anthraquinone
BBD	Box-Behnken Design
CCD	Composite central design
DOE	Design of Experiments
FFD	Full Factorial design
FST	Faculty of Sciences and Technology
HeF	Heterogenous Fenton
RSM	Response Surface Methodology
SFs	Spinel ferrites
SHS	self-propagating high-temperature synthesis
STEVA	Science and Technology of Environment and Valorization

Abstract

الملخص

يتناول هذا البحث إزالة صبغة "الأخضر الحمضي 25" من نوع الأنثراكينون، باستخدام نانوفيريتات من فيريت النحاس عبر عملية فنتون غير متجانسة تُنفذ في الظلام. يهدف هذا العمل إلى تقييم فعالية هذه المحفزات النانوية في معالجة مياه الصرف الصناعي، مع تحسين ظروف التشغيل باستخدام تصميم مركب مركزي ضمن منهجية الاستجابة السطحية.

تمت دراسة تأثير المتغيرات الأساسية مثل كمية المحفز، وتركيز بيروكسيد الهيدروجين، وزمن التفاعل. أظهرت النتائج أن الشروط المثلى (0.5 غرام لكل لتر من فيريت النحاس، 3 مليمول لكل لتر من بيروكسيد الهيدروجين، لمدة 60 دقيقة) قد حققت نسبة إزالة للون بلغت حوالي 98.6 بالمئة.

النموذج الإحصائي المستخدم) التصميم المركب المركزي (Central Composite Design – أظهر دقة تنبؤية عالية، مما يؤكد موثوقيته. كما أظهرت الدراسة قابلية المحفز لإعادة الاستخدام مع ثبات كفاءته، مما يجعله خياراً فعالاً ومستداماً لمعالجة المياه الملوثة بالأصباغ.

الكلمات المفتاحية: الأخضر الحمضي 25، نانوفيريتات، فنتون غير متجانس، معالجة المياه، التصميم التجريبي.

Abstract

This research focuses on the degradation of the anthraquinone dye Acid Green 25 (AG25) using CNF400 nanoferrites through a heterogeneous Fenton-like process conducted in the dark. The objective is to evaluate the effectiveness of these nanocatalysts in wastewater treatment and to optimize the process parameters using Central Composite Design (CCD) under the Response Surface Methodology (RSM). The influence of key variables such as catalyst dose, hydrogen peroxide concentration, and reaction time was studied. The optimal operating conditions (0.5 g/L catalyst, 3 mM H_2O_2, and 60 minutes reaction time) led to a decolorization efficiency of 98.6%. The CCD model demonstrated strong predictive performance ($R^2 = 0.9973$), confirming its reliability. The reusability and stability of the catalyst across multiple cycles highlight its potential as an effective and sustainable solution for dye-contaminated wastewater treatment.

Keywords: Acid Green 25, nanoferrites, heterogeneous Fenton process, wastewater treatment, Central Composite Design, dye degradation.

Résumé

Ce travail porte sur la dégradation du colorant anthraquinonique Vert Acide 25 (AG25) à l'aide de nanoferrites de ferrite (CNF400) via un procédé Fenton hétérogène réalisé dans l'obscurité. L'objectif est d'évaluer l'efficacité de ces nanocatalyseurs dans le traitement des eaux usées et d'optimiser les paramètres du processus en utilisant le plan d'expérience Central Composite Design (CCD) dans le cadre de la méthodologie des surfaces de réponse (RSM). L'influence de variables clés telles que la dose de catalyseur, la concentration de peroxyde d'hydrogène et le temps de réaction a été étudiée. Les résultats ont montré que les conditions optimales (0,5 g/L de catalyseur, 3 mM H_2O_2, 60 minutes temps de reaction) permettent d'atteindre un taux de décoloration allant jusqu'à 98,6 %. Le modèle CCD a montré une performance prédictive remarquable (R^2 = 0,9973), confirmant sa fiabilité. La réutilisabilité et la stabilité du catalyseur sur plusieurs cycles démontrent son potentiel comme solution efficace et durable pour le traitement des eaux colorées.

Mots-clés : Vert Acide 25, nanoferrites CNF400, procédé Fenton hétérogène, traitement des eaux usées, plan d'expérience CCD, dégradation des colorants.

Table

General introduction

Preserving water quality is paramount, necessitating effective treatment systems to eliminate contaminants such as synthetic dyes [1]. These pollutants notably anthraquinone dyes like Acid Green 25 (AG25) exhibit toxic, mutagenic, carcinogenic, and allergenic properties that pose significant risks to human health [2]. Regulatory concerns about AG25's environmental persistence [3] underscore the urgent need for cleaner, energy-efficient, and cost-effective water treatment technologies. Advanced Oxidation Processes (AOPs), particularly the Fenton process, offer promising eco-friendly solutions due to their high efficiency, operational simplicity, and low toxicity [4,5].

This study conducted within the framework of Dr. Bendahman Rachida's doctoral research investigates nanoferrite-enhanced Fenton-like processes for AG25 removal from aqueous solutions. Given AG25's extensive use in textiles and cosmetics, we evaluate the adsorption capacity, degradation efficiency, and sustainability of this approach using nanoferrite catalysts. Our goals are threefold:

1) Optimize degradation kinetics for recalcitrant dyes
2) Develop cost-effective remediation strategies
3) Establish green alternatives for industrial wastewater treatment

This dissertation comprises a general introduction, two main research chapters, a general conclusion with recommendations, along with supporting appendices and references.

Chapter I, the literature review, examines key themes including water pollution, the characteristics and environmental impacts of industrial dyes (specifically anthraquinone-based dyes), and contemporary wastewater treatment technologies. It details the Fenton process, including its mechanisms, and explores the application of nanotechnology, with a focus on spinel ferrite nanoparticles. This chapter also covers the chemical and green synthesis methods for these nanoparticles and introduces the statistical optimization techniques employed in this study, namely Response Surface Methodology (RSM) using Central Composite Design (CCD).

Chapter II presents the experimental component of the research. It describes the preparation of CNF400 nanoferrites and their application in the dark Fenton degradation of Acid Green 25 (AG25) dye. This chapter details the materials, analytical techniques, and experimental methodology used to investigate the effects of critical parameters such as catalyst concentration and temperature, as well as catalyst reusability. The results are thoroughly discussed to evaluate the effectiveness of the CNF400-based treatment and the viability of the optimization approach

Chapter I :

Literature Review

I.1 Introduction:

Water pollution, caused by various organic contaminants in surface and groundwater, poses serious environmental and human health risks, making it a key concern in scientific research [6]. These pollutants, mainly from industrial and residential sources, include hazardous substances and biological waste that can have irreversible effects on ecosystems. Traditional wastewater treatment methods, although widely used, are often limited in their effectiveness [7]. In response to these challenges, there is a growing need for cost-effective and energy-efficient technologies**.** Nanotechnology has emerged as a promising solution, offering innovative and multifunctional materials that can treat water from both conventional and unconventional sources [8]. With their high surface area, ease of functionalization, and reactivity, nanomaterials can effectively remove a broad spectrum of contaminants, including heavy metals, dyes, and organic/inorganic pollutants [9].

I.2 Water pollution

I.2.1 Overview of Water Pollution

Water pollution primarily stems from industrial and agricultural activities, certain natural phenomena, and the lack of adequate water and wastewater infrastructure. Among these, industrialization remains the most impactful contributor. Sectors such as distilleries, tanneries, pulp and paper, textiles, food processing, steel manufacturing, and nuclear energy are major polluters.

These industries release a range of contaminants, including toxic substances, organic and inorganic compounds, hazardous solvents**,** and volatile organic compounds (VOCs)**.** When

discharged untreated into aquatic ecosystems, these pollutants lead to significant environmental degradation [10].

Persistent organic pollutants (POPs) are particularly problematic in the 21st century, disrupting the global water cycle. Contaminated water not only threatens public health and ecological stability, but also has socio-economic impacts. Emerging pollutants such as dyes, pharmaceuticals, agrochemicals, and landfill leachates can cause environmental damage even at trace concentrations [12].

In light of these risks, international environmental regulations increasingly mandate that industries pre-treat or fully treat their effluents before discharge, to avoid long-term harm to aquatic life and ecosystems [11].

I.2.2 Dyes

Synthetic dyes represent a major environmental concern due to their extensive industrial usage [13] and the large volumes discharged into wastewater. Historically, natural dyes—derived from minerals, plants, or animals (e.g., turmeric, henna, onion peel)—were widely used. However, their limited availability and inability to meet industrial-scale demand have led to their replacement by synthetic dyes [14].

Today, synthetic dyes are employed in textiles, paper, leather, plastics, pharmaceuticals, cosmetics, and food industries. Over 100,000 types of dyes are commercially available, with global production exceeding 700,000 tons per year, approximately two-thirds of which is consumed by the textile sector [15].

In the textile industry, dyeing and printing processes require between 120–280 liters of water per kilogram of fabric, and rely heavily on petroleum-derived dyes [16-17]. However, an estimated 11–15% of dyes fail to bind to fibers and are directly released into effluents, contributing to elevated chemical oxygen demand (COD) and biological oxygen demand (BOD).

These unbound dyes are highly stable, poorly biodegradable, and resistant to conventional treatments [16]. Once released into aquatic environments, they severely reduce light penetration, inhibiting photosynthesis, and contribute to oxygen depletion, which can be fatal for aquatic life [18].

Dyes are generally classified into natural and synthetic categories, with synthetic dyes further divided into several chemical families (see Table I.1) [19, 14]. Despite their advantages in terms of color strength, cost, and performance, many synthetic dyes especially those based on anthraquinone or azo structures pose risks due to their toxicity, persistence, and potential carcinogenicity [19]. Figure I-1 represents applications of Natural and synthetic dyes.

Table I-1 : Chemical Classes and Structures of Natural and Synthetic Dyes

Natural Dyes [19]		**Synthetic dyes** [20]	
Chemical Classes	**Structure**	**Chemical Classes**	**Structure**
Indigoids	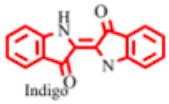 Indigo	Azo	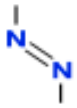
Berberine	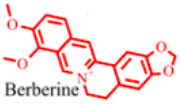 Berberine	Anthraquinone	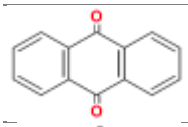
Carotenoids	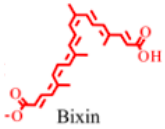 Bixin	Triphenylmethane	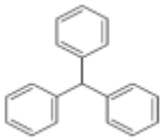
Flavonoids	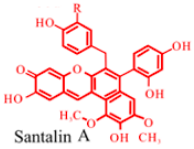 Santalin A	Nitro and Nitroso	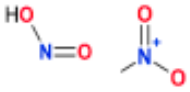
Dihydropyran based	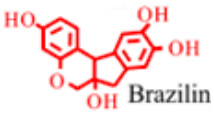 Brazilin	Indigoid	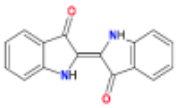
Betalain	 Betacyanin	Xanthene	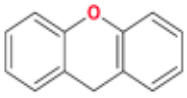
Tannins	 Chebulic acid	Acridine	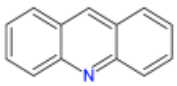

Quinonoids

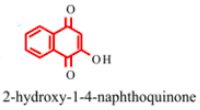

2-hydroxy-1-4-naphthoquinone

Phthalein

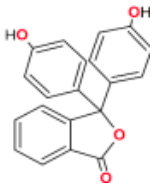

Figure I-1 : Multifunctional Applications of Natural and Synthetic Dyes [22]

I.2.3 Anthraquinone

Anthraquinones (AQs) belong to a broader class of compounds known as quinones, which include benzoquinones, naphthoquinones, and anthraquinones [13] (see Figure I.2). Structurally, anthraquinones are characterized by a 9,10-dioxoanthracene core, which imparts significant chemical stability and redox activity.

Naturally occurring in a variety of plants, AQs have been traditionally used as pigments, laxatives, and antibacterial or anti-inflammatory agents. More recently, derivatives of anthraquinone have found applications in the treatment of conditions such as constipation, arthritis, multiple sclerosis, and even certain cancers [23].

Their widespread use also extends to the dye and textile industries, where anthraquinone-based compounds are valued for their vivid color, chemical resistance, and photostability. However, these same features make them highly persistent in wastewater, especially in textiles effluents.

Due to their ability to participate in electron transfer reactions, anthraquinones are also studied in electrochemical applications, including as redox mediators in the anaerobic bioreduction of heavy metals and organic pollutants, and as electrode materials in supercapacitors and lithium-ion batteries [12].

Despite their versatility, many anthraquinone dyes raise environmental and health concerns. Their aromatic stability makes them recalcitrant to biodegradation, and some have been identified as potentially mutagenic or carcinogenic. While the toxicology of azo dyes has been extensively studied, research on the biotransformation and ecotoxicity of anthraquinones remains relatively limited and warrants further investigation [20].

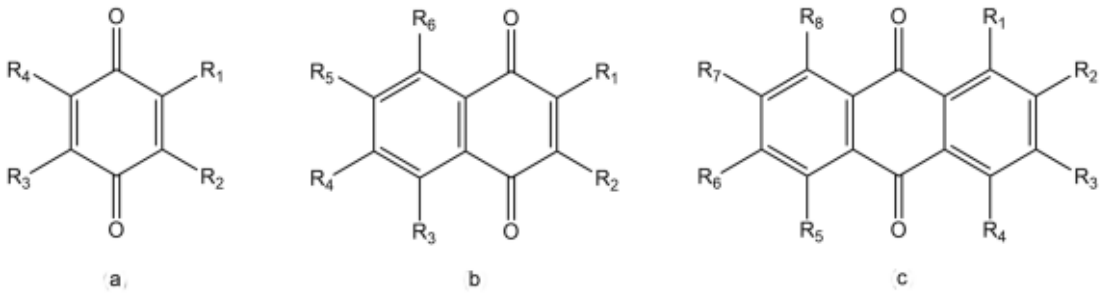

Figure I-2 : Chemical structure of a benzoquinone, b naphthoquinone and c anthraquinone [23]

I.2.4 Environmental Effects of Industrial Dyes

Synthetic dyes, due to their complex aromatic structures and physicochemical stability, are generally non-biodegradable. Their persistence in aquatic environments leads to a series of ecological and health-related issues. Many synthetic dyes have been classified as toxic, mutagenic, or carcinogenic, and can accumulate in organisms through bioaccumulation and biomagnification, affecting upper trophic levels.

A critical factor is that environmental harm is not solely dependent on the quantity of dyes released, but also on their chemical composition, concentration, and interaction with other contaminants in industrial effluents. For instance, synergistic effects between dyes and heavy metals or organic solvents can significantly amplify toxicity.

Once released into water bodies, dyes absorb visible light, leading to a reduction in sunlight penetration. This disrupts photosynthesis in aquatic plants and algae, lowers dissolved oxygen levels, and induces hypoxic conditions that can be fatal to aquatic organisms.

Additionally, dyes can impair soil quality when present in irrigation water or sludge, affecting microbial activity and plant growth. Some dyes have been reported to persist for decades, with half-lives extending up to 50 years in anaerobic conditions [20].

These risks have prompted increased regulatory pressure on industries to pre-treat or eliminate dyes from wastewater before discharge [20]. Consequently, the development of efficient, cost-effective, and environmentally friendly treatment technologies has become a research priority.

These environmental and biological impacts are summarized in Figure I.3, which illustrates the main pathways of dye-induced harm in aquatic and terrestrial ecosystems.

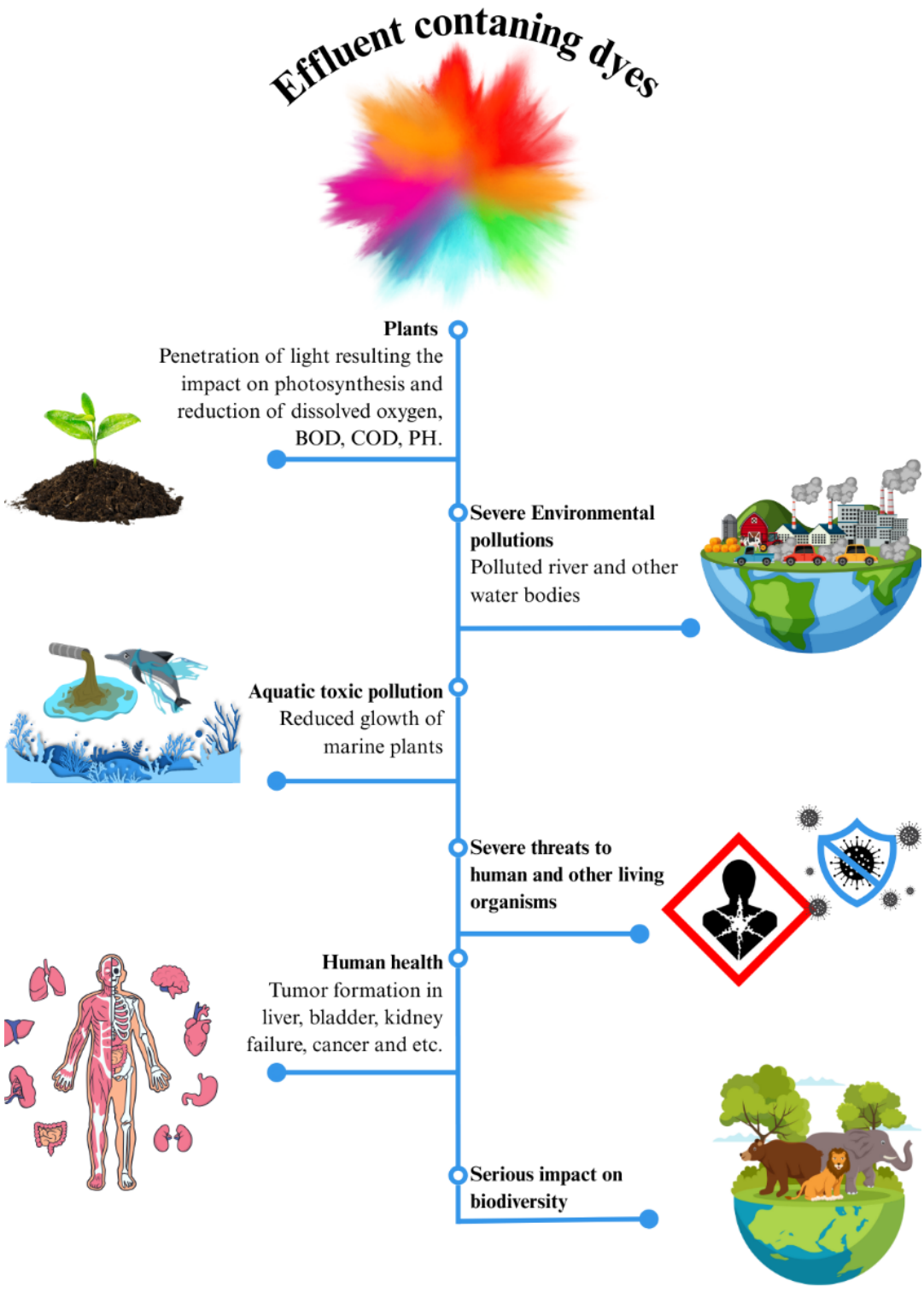

Figure I-3 : Environmental and Health Hazards of Dye-Contaminated Effluents [24]

I.3 Treatment technology for dye-containing effluent

Dye removal employs three primary approaches: biological, chemical, and physical methods (Figure I-4). However, due to the complexity of dye-laden effluents, none of these methods alone is fully effective [15]. Chemical treatments (e.g., flocculation/coagulation, ion exchange), while efficient, face notable drawbacks including secondary pollution from reagent overuse, concentrated sludge generation, and high costs limiting large-scale application.

To address these limitations, advanced oxidation processes (AOPs) such as ozonation, Fenton reaction, UV/hydrogen peroxide, and photocatalysis have emerged as promising alternatives [13]. AOPs generate highly reactive oxidants (e.g., hydroxyl radicals) capable of non-selectively degrading diverse ionic and non-ionic dyes, enabling rapid mineralization of complex organics. Their advantages include high degradation efficiency, broad applicability across wastewater types, and operational flexibility.

Table I.2 provides a comparative overview of conventional chemical treatments and AOPs, detailing their respective advantages and disadvantages.

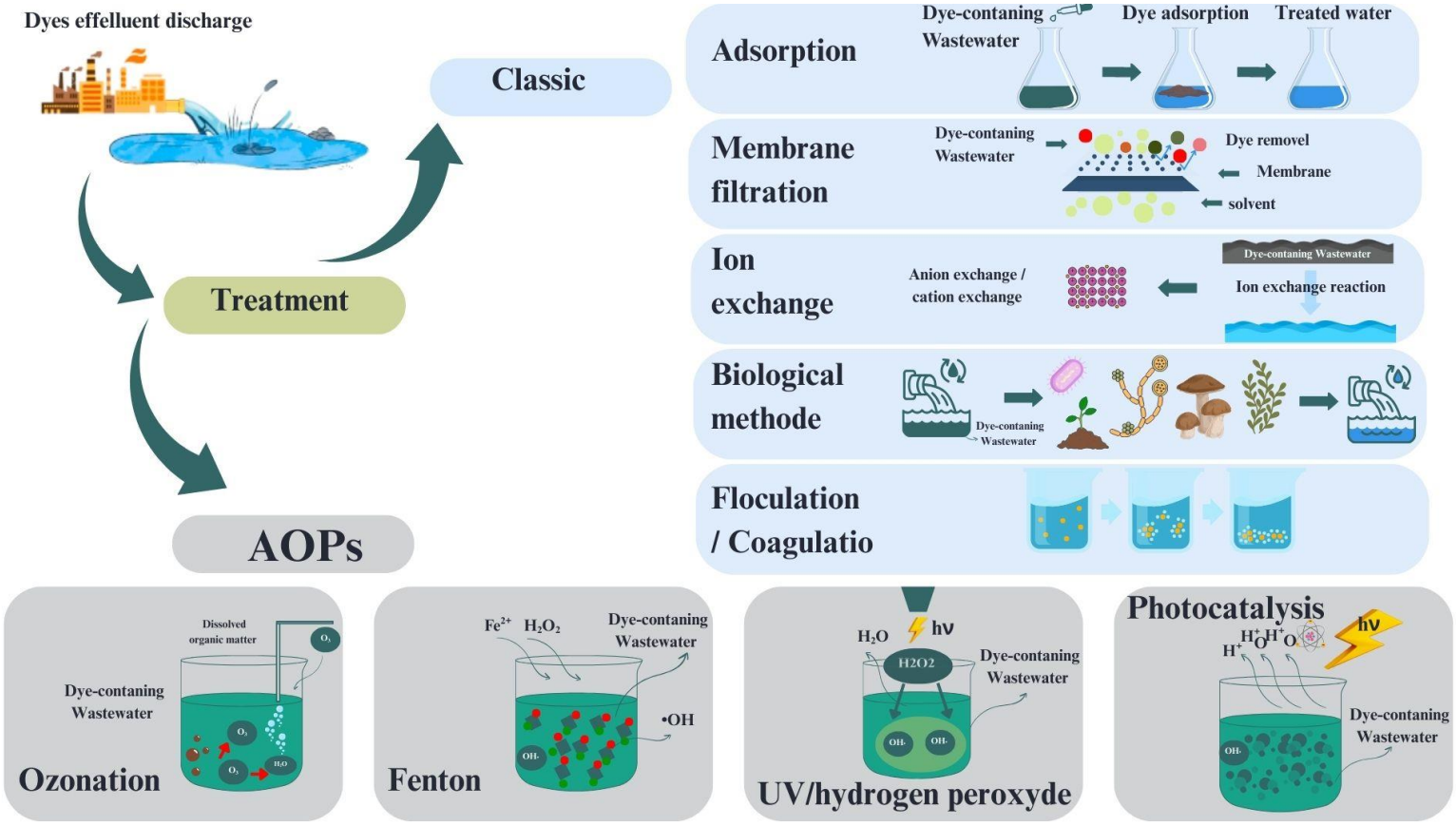

Figure I-4 : Classical and Advanced Strategies for the Treatment of Industrial Dye Effluents [21,25-28].

Table I-2 : Different Methods for Removing Dyes from Wastewater

Methods		Advantages	Disadvantages	Ref
Classic	Adsorption	- Low operational cost - Good dye removal efficiency - Short reaction time	- Challenge in regeneration of adsorbents - Generates toxic by-products: no mineralization of dyes - Not applicable to all dyes - - Requires precise control of process conditions e.g pH - The high cost of some activated carbon	[2,25]
	Membrane filtration	- resistance to temperature, chemical toxicity and microbial attack - Environmentally friendly: no chemicals are used - Easily applicable in actual industrial applications	- high start-up costs - clogging and membrane upkeep. - Poor dye mineralization	[2,13]
	Ion Exchange	- High cation exchange capacity - The elimination of toxic and soluble pollutants	- high cost - Not suitable for all dyes	[30,31]
	Flocculation/ Coagulation	- Simple and economical. - Good dye removal efficiency	- Some chemicals are toxic, sludge generation - Requires precise control of process conditions e.g. pH	[25,20]
	Biological Methods	- High removal of biochemical oxygen demand and suspended solids - Simple, economically attractive and environmentally friendly process	- Requires optimally favorable environment - Requires management and maintenance of the microorganisms and/or physicochemical pre-treatment - Slow process - Generation of biological sludge and uncontrolled degradation products	[25]
AOPs	Ozonation	- no sludge produced - Easy industrial application (on-site treatment)	- High cost of electricity required	[2,20,13]
	Fenton	- For both soluble and insoluble dyes, this technique works well. - All contaminants in water are removed Suitable for dye wastewater including solids	- Disperse and vat dyes cannot be removed. - Iron sludge production is high. - Long reaction time	[13]
	UV Hydrogen Peroxide	- Easy handling, high stability - Availability of H_2O_2 - no sludge formation and high-rate mineralization	- Producing aromatic chemicals, which can be harmful to human health and the environment - Costly and undesirable products are generated.	[20,29]
	Photocatalysis	- Effective oxidation and lab scale applicability - No sludge generation	- Formation of by-products Excessive dissolved O_2 is required	[31]

I.3.1 Principle and mechanism of Fenton processes

The Fenton process ranks among the most effective and cost-efficient advanced oxidation techniques for degrading organic pollutants in aqueous environments. It operates through the catalytic reaction between hydrogen peroxide (H_2O_2) and ferrous ions (Fe^{2+}) under acidic conditions, generating highly reactive hydroxyl radicals ($HO^{\bullet}$) that oxidize diverse contaminants. This method has proven successful in treating industrial and municipal effluents containing persistent organic compounds and pesticides, and shows potential for certain heavy metal oxidation [29].

However, the conventional homogeneous Fenton process faces significant limitations: narrow operational pH range (typically 2.5-3.5), continuous iron consumption requiring catalyst replenishment, formation of iron sludge complicating disposal, and catalyst deactivation. To overcome these constraints, research has shifted toward heterogeneous Fenton-like systems [29], which offer enhanced catalyst stability, wider pH tolerance, and simplified recovery/reuse.

I.3.1.1 Homogeneous Fenton process

As demonstrated in figure I-5, the Fenton reagent, composed of ferrous ions (Fe^{2+}) and hydrogen peroxide (H_2O_2), produces highly reactive species, primarily hydroxyl radicals (•OH), as illustrated in Equation (I.1). This reaction initiates a powerful oxidation process responsible for the degradation of organic pollutants. In addition to this primary reaction, a termination step occurs, as shown in Equation (I.2), which limits radical propagation. A Fenton-like mechanism can also take place when ferric ions (Fe^{3+}) react with hydrogen peroxide, leading to its decomposition into reactive intermediates, as depicted in Equation (I.3).

Moreover, the Fenton process involves a series of complex secondary reactions, represented in Equations (I.4)–(I.7), which illustrate the chain reactions contributing to the overall efficiency of pollutant degradation [33]:

$$Fe^{2+} + H_2O_2 \rightarrow Fe^{3+} + \bullet OH + OH^- \quad \text{I-1}$$

$$Fe^{2+} + \bullet OH \rightarrow OH^- + Fe^{3+} \quad \text{I-2}$$

$$Fe^{3+} + H_2O_2 \rightarrow Fe{-}OOH^{2+} + H^+ \quad \text{I-3}$$

$$Fe{-}OOH^{2+} \rightarrow HO^{\cdot}{}_2 + Fe^{2+} \quad \text{I-4}$$

$$Fe^{2+} + HO_2^{\cdot} \rightarrow HO_2^{-} + Fe^{3+} \quad \text{I-5}$$

$$Fe^{+3} + HO_2^{\cdot} \rightarrow Fe^{+2} + O_2 + H^{+} \quad \text{I-6}$$

$$\bullet OH + H_2O_2 \rightarrow H_2O + HO_2^{\cdot} \quad \text{I-7}$$

As illustrated in Equation (I.8), a simplified version of the Fenton reaction has been proposed as an alternative to the series of complex reactions previously described. It is evident that acidic conditions (presence of H^+ ions) enhance the efficiency of the Fenton process [33]:

$$Fe^{2+} + H_2O_2 + H^{+} \rightarrow Fe^{3+} + \bullet OH + H_2O \quad \text{I-8}$$

Equation (I.9) demonstrates the chain oxidation reactions in which organic compounds react with hydroxyl radicals (•OH), forming organic radicals that are subsequently converted into final oxidized products [33]:

$$RH + \bullet OH \rightarrow H_2O + R^{\cdot} \rightarrow Oxidized\ product \quad \text{I-9}$$

The homogeneous Fenton process involves three fundamental steps: (1) dissolution of the catalyst, (2) generation of hydroxyl radicals (•OH), and (3) oxidation of organic compounds. Once the iron catalyst dissolves, Fe^{2+} ions react with hydrogen peroxide to generate •OH radicals, which are primarily responsible for pollutant degradation. The efficiency of this process is largely governed by the concentrations of both the catalyst and the oxidant. However, exceeding the optimal concentrations of either component can lead to radical scavenging reactions, thereby reducing the availability of •OH and ultimately decreasing the overall efficiency of the treatment [33].

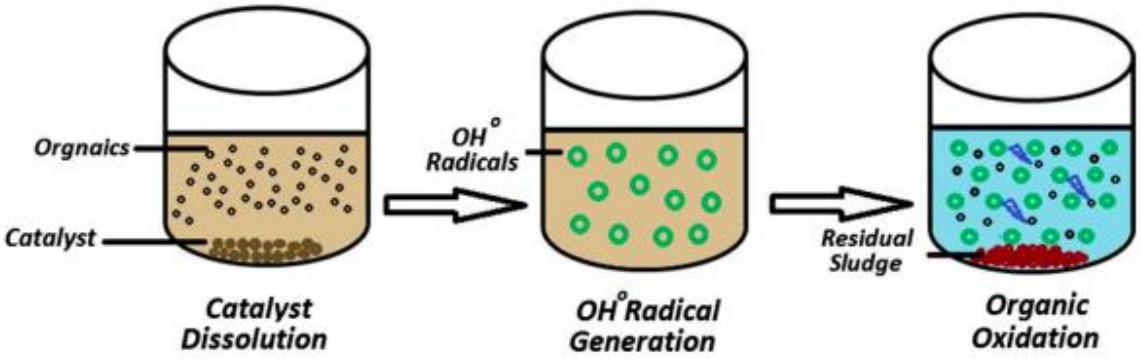

Figure I-5 : Three main steps of the homogeneous Fenton process [33].

I.3.1.2 Heterogeneous Fenton-like reaction

Heterogeneous Fenton-like (HeF) processes have emerged as a promising alternative to conventional Fenton systems, addressing key limitations [29,34]. By utilizing solid catalysts instead of dissolved ferrous ions, HeF systems significantly reduce iron-containing sludge generation. This advantage stems from controlled iron leaching: unlike homogeneous systems where rapid iron dissolution produces substantial sludge, the slow leaching kinetics of solid catalysts minimize sludge formation, eliminating post-treatment needs and reducing environmental impact.

The solid-phase design enhances sustainability through catalyst recoverability and reusability. Low iron leaching directly improves cost-effectiveness and environmental compatibility, while studies confirm that most HeF catalysts maintain structural and catalytic stability over multiple cycles a critical factor for practical implementation. Among explored materials, nanostructured ferrites exhibit particular promise due to their unique physicochemical properties and high performance in Fenton-like reactions.

Mechanistically, HeF reactions proceed through hydrogen peroxide activation at surface active sites (AS), as described in Equations (I.10-I.11) [34].

$$AS - Fe^{+2} + + H_2O_2 \rightarrow AS - Fe^{3+} + HO^- + \bullet OH \quad \text{I-10}$$

$$\mathrm{AS - Fe^{3+} + H_2O_2 \rightarrow AS - Fe^{2+} + HO_2\bullet + H^+} \quad \text{I-11}$$

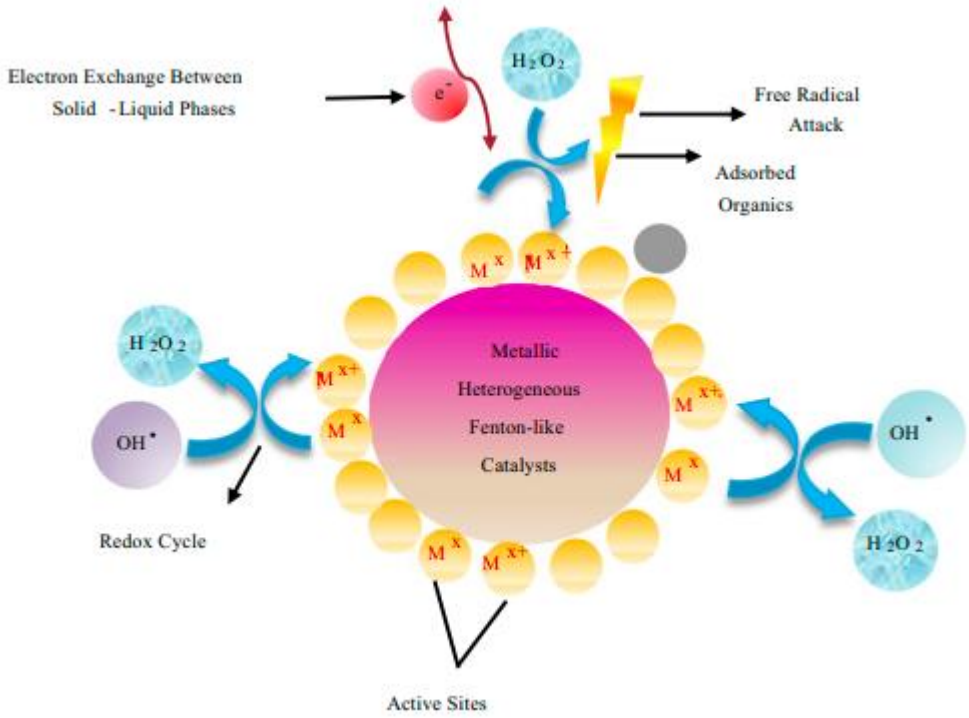

Figure I-6 : Heterogeneous Fenton-like oxidation process [33].

I.3.2 Mechanism of free radical

The efficiency of Advanced Oxidation Processes (AOPs) hinges critically on the generation and reactivity of radical species. Precise identification and quantification of key radicals—including $SO_4^{\bullet-}$, •OH, $SO_3^{\bullet-}$, $O_2^{\bullet-}$, and $^1O_2$ are thus fundamental to understanding and optimizing oxidative degradation mechanisms.

In H_2O_2-driven systems, a dynamic equilibrium exists between •OH, $O_2^{\bullet-}$, and $^1O_2$. A pivotal pathway involves hydroperoxyl radical ($HO_2^{\bullet}$) formation via •OH-mediated H_2O_2 oxidation. This $HO_2^{\bullet}$ intermediate subsequently initiates radical interconversion cascades, generating secondary •OH, $O_2^{\bullet-}$, and $^1O_2$ species (figure I-7). These complex transformations govern both the efficacy and mechanistic intricacy of radical-based degradation pathways [14].

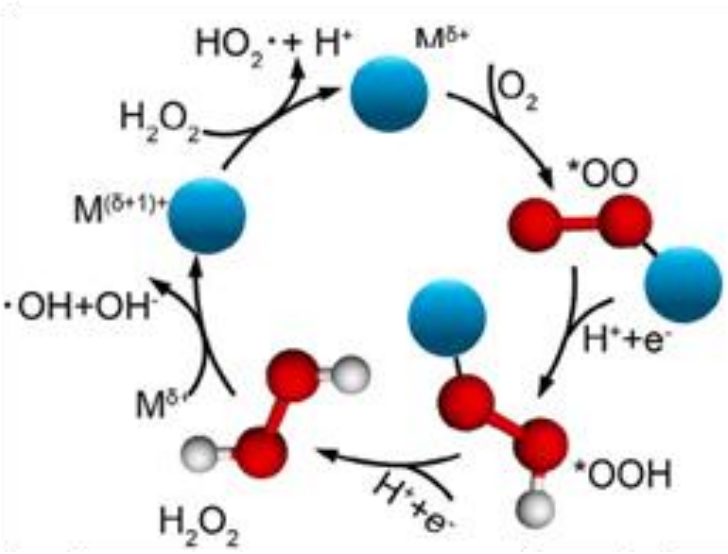

Figure I-7 : Mechanism of Hydrogen Peroxide Formation and Degradation via Metal-Catalyzed Redox Cycling [14].

I.4 Nanotechnology in Wastewater Treatment

I.4.1 Introduction to Nanotechnology

Recent advances in nanoscale engineering have enabled the design of functional materials with precise geometric control and tailored surface properties. These engineered nanoparticles have become pivotal across multiple disciplines particularly in catalysis due to their exceptionally high surface-to-volume ratios. As particle dimensions decrease, the density of accessible active sites increases exponentially, dramatically enhancing reactivity and application potential [35]. Among nanomaterials for heterogeneous Fenton catalysis, spinel demonstrate exceptional promise. Their advantages include:

- Earth abundance and low-cost synthesis
- Enhanced catalytic activity from surface oxygen mobility and defect sites
- Robust stability (thermal/chemical/mechanical)
- Facile magnetic recovery enabling practical reuse
- Tunable electronic properties influencing reaction pathways

These combined characteristics make ferrites ideal catalysts for environmental remediation, particularly where separation efficiency and long-term stability are critical [12].

I.4.2 Spinel-type nanoparticles (Nano-spinel)

The spinel ferrites as highly attractive materials for sustainable environmental remediation strategies and other catalytic applications [12]. Their large specific surface area, high surface oxygen mobility, and selective reactivity make them particularly effective in advanced oxidation processes.

Spinel ferrites (SFs) spinel ferrites with the general formula MFe_2O_4 (where M = Fe, Co, Ni, Mn, Mg, Cu, Zn, etc.) are categorized into three models depending on the degree of inversion with respect to the cation distribution of M^{2+} and Fe^{3+} ions at both the tetrahedral (A) and octahedral (B) sites. The degree of inversion is specified by a value represented by x, which is the fraction of M^{2+} ions occupying the octahedral site. The overall composition can be represented by the general formula: $M^{2+}{}_{1-x}Fe^{3+}{}_{x}Fe^{3+}{}_{2-x}M^{2+}{}_{x}$, which is a standard descriptor of cationic disorder [12].

- When x = 0, the structure is known as normal spinel because the divalent cations (M^{2+}) occupy the tetrahedral site (A) whilst the trivalent cations (Fe^{3+}) occupy octahedral sites (B) in the spinel structure.
  Structural formula: $M^{2+}Fe^{3+}{}_2O_4$
  Examples: $ZnFe_2O_4$, $CdFe_2O_4$ [12]
- When x = 1, it is termed inverse spinel, in which the divalent cations (M^{2+}) occupy the octahedral sites (B), whilst the trivalent cations (Fe^{3+}) occupy both the tetrahedral (A) and the octahedral (B) sites equivalently.
  Structural formula: $Fe^{3+}M^{2+}Fe^{3+}O_4$ [12]
  Examples: Fe_3O_4, $CoFe_2O_4$, $NiFe_2O_4$, $CuFe_2O_4$, $MgFe_2O_4$.
- When $0 < x < 1$, the structure is defined as mixed spinel where both M^{2+} ions and Fe^{3+} ions are distributed between the tetrahedral (A) and octahedral (B) sites.
  Example: $MnFe_2O_4$ [12].

I.4.3 Synthesis methods of spinel ferrites nanoparticles

I.4.3.1 Co-precipitation

Co-precipitation produces spinel ferrites by concurrent precipitation of metal ions from homogeneous salt solutions. Crystal growth/agglomeration are controlled by salt concentration, temperature, pH, and pH adjustment rate. The solid is then collected, washed, and thermally dried. [36].

I.4.3.2 Sol-gel

The sol-gel method synthesizes metal oxide nanostructures via metal alkoxide dissolution in water/alcohol, followed by hydrolysis, gelation, drying, and calcination to remove organics [37].

I.4.3.3 Autocombustion

Combustion synthesis (SHS) economically produces pure, uniform nanocrystalline powders. This wet chemical method prepares a metal salt/fuel aqueous gel, then ignites it to yield high-surface-area porous oxides. [37].

I.4.4 Green synthesis of nanoparticles

Green synthesis methods now widely produce size/shape-controlled nanoparticles using plant extracts. Their natural compounds reduce metal cations, leveraging botanical diversity to tune nanoparticle properties [38]. The four methods are illustrated in Figure 8.

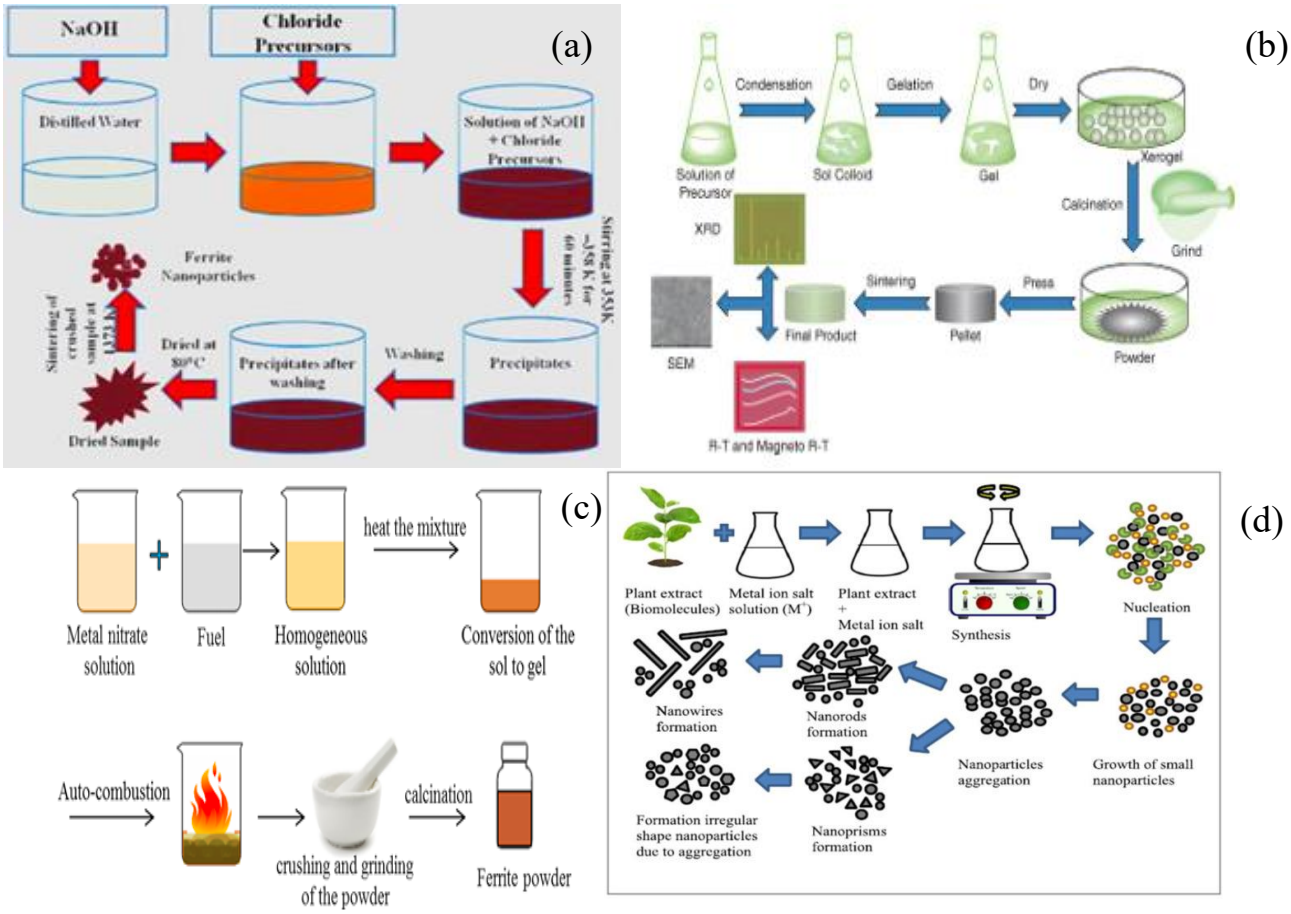

Figure I-8 : Different synthesis methods, a) Co-precipitation, b) Sol gel, c) Autocombustion, d) Green synthesis [37,12,39]

I.5 RSM

Response Surface Methodology (RSM) is a robust statistical tool for optimizing complex processes with interacting variables. It simultaneously evaluates individual (main) and combined (interaction) effects through structured experimental designs [40,41], enabling precise identification of optimal operational conditions. RSM's versatility facilitates data manipulation, analysis, and interpretation, ensuring high reproducibility and process improvement [42].

Figure 9 outlines the systematic Design of Experiments (DOE) workflow, spanning factor identification to optimization/validation. Widely used designs include Full Factorial (FFD), Central Composite (CCD), and Box-Behnken (BBD). Here, factors are independent variables

influencing system outcomes, while levels represent their experimental settings. Accurate level definition is essential for probing variable interactions across the experimental domain [43].

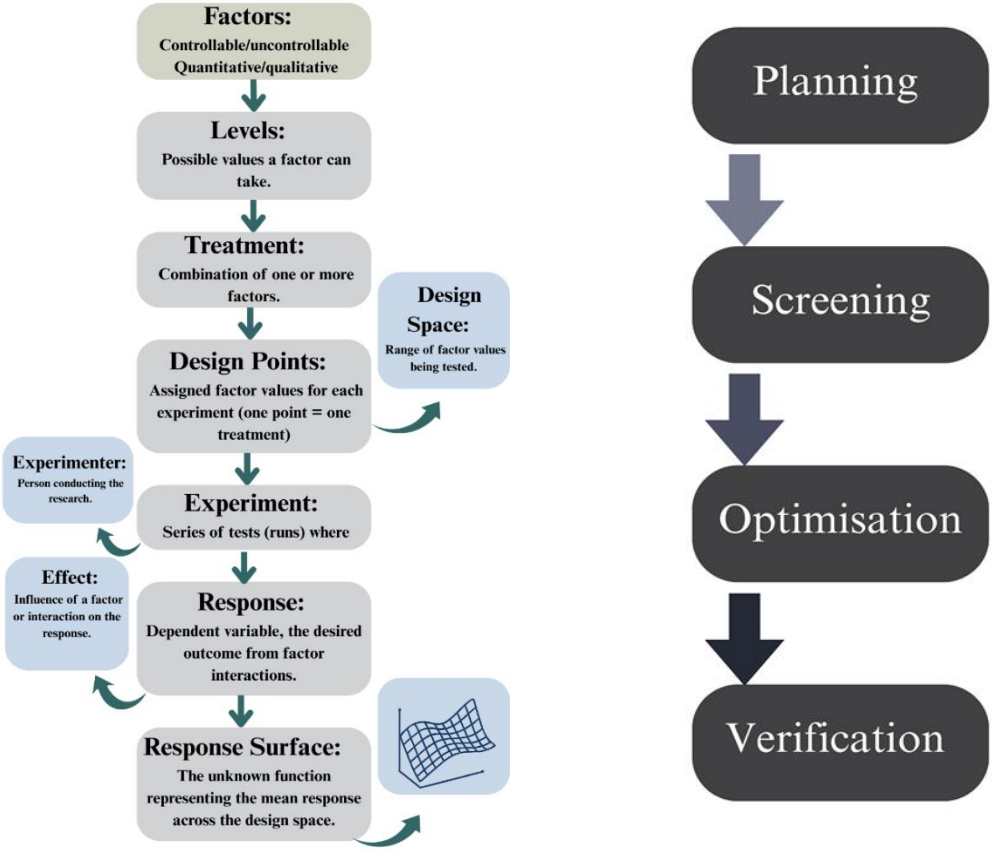

Figure I-9 : Systematic approach to the Design of Experiments (DOE) [43,44]

I.5.1 Central composite design (CCD)

The Central Composite Design (CCD), a premier response surface methodology, efficiently expands factorial experiments by incorporating axial and center points (Figure I.10). Its structure comprises:

- 2^n factorial runs
- 2n axial runs (ensuring design rotatability)
- n_a center runs (quantifying experimental error and data reproducibility)

Axial points maintain uniform prediction variance at equidistant locations from the design center [44]. Key advantages of CCD versus other RSM approaches are summarized in Table I.3. The total number of experimental runs is calculated using the following equation:

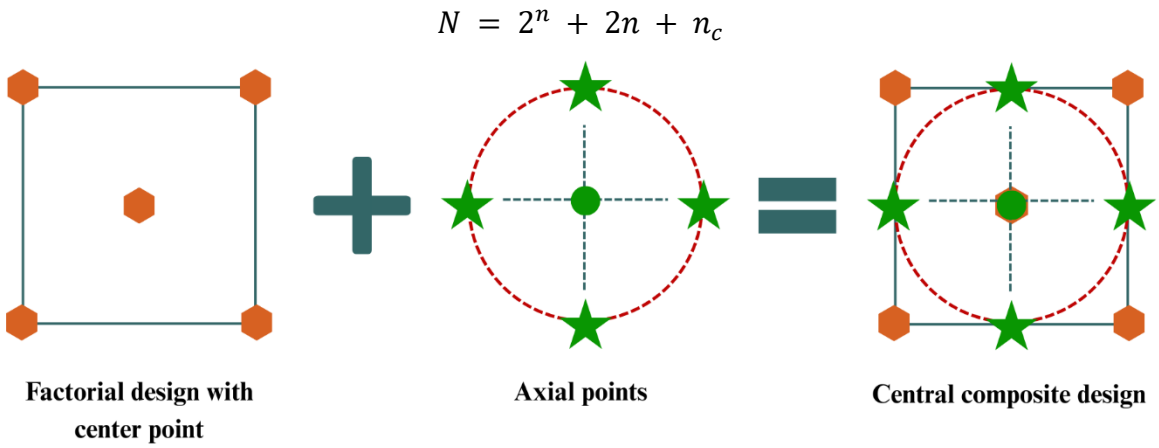

Figure I-10 : CCD graphical representation, reproduced [43]

Table I-3 : Advantages of RSM and CCD [44,45]

Advantages of RSM	Advantages of CCD
• Smooth statistical analysis • Improving a production system, procedure, or end product. • Design and layout for experiments. • Forecasting • Clear curves and other visual aids make it simple to illustrate how variables interact. • Effective response or outcome visualization using surface plots, graphs, etc. • Related mathematical frameworks for empirical data.	• It turns out to be the extension of 2 level factorial or fractional factorial design • To estimate nonlinearity of responses in the given data set • Helps to estimate curvature in obtained continuous responses • Maximum information in a minimum experimental trial

I.6 Overview of Applications of Fenton process in dye degradation

I.6.1 Statistical modeling and optimization of heterogeneous Fenton-like removal of organic pollutant using fibrous catalysts: a full factorial design

This study optimized heterogeneous Fenton-like dye degradation using polyester-supported zerovalent iron catalysts functionalized with various groups. A full factorial design (L_{27}) assessed pH and H_2O_2 concentration effects (95% confidence). Results revealed:

- Dye removal efficiency decreased above pH 5
- H_2O_2 concentration enhanced degradation until equilibrium
- Catalyst type showed no statistical significance
- ANOVA confirmed synergistic pH/ H2O2 interaction

Functionalization was verified by electrokinetic analysis and X-ray photoelectron spectroscopy (XPS). This optimization enables scalable, eco-friendly catalyst design for wastewater treatment [46]

I.6.2 Challenges and Advances in Dye Removal Using IONzyme-Based Catalysts: Expanding the Scope of Heterogeneous Fenton-like Processes

Here, heterogeneous Fenton-like processes were explored for decolorization of dye with IONzyme-based catalysts—enzyme-like iron oxide nanoparticles. Focus was on maximizing catalytic activity and durability by surface modification, magnetite replacement with other metals, and support from biomass. The IONzymes showed promising results in azo and anthraquinone dye degradation under a synergistic process combining adsorption and Fenton-like oxidation. However, the problem of acidic pH requirements, catalyst deactivation, metal leaching, and processing of spent materials are remaining significant obstacles to widespread application [47].

I.6.3 Green synthesis of iron nanoparticles using Artocarpus heterophyllus peel extract and their application as a heterogeneous Fenton-like catalyst for the degradation of Fuchsin Basic dye

Iron nanoparticles (Fe NPs) were green-synthesized using jackfruit peel extract as bioreductant/stabilizer, valorizing agro-waste per green chemistry principles. The 33 nm NPs (zero-valent iron/oxides), characterized by TEM/SEM-EDX, XRD, and FTIR, achieved 87.5% Fuchsin Basic dye degradation in 20 min at 318 K. Kinetic analysis revealed pseudo-first-order, surface reaction-controlled catalysis, confirming effective active sites [48].

I.6.4 Metallic nickel nanoparticles supported polyaniline nanotubes as heterogeneous Fenton-like catalyst for the degradation of brilliant green dye in aqueous solution.

Novel magnetic PANI/Ni^0 nanocomposites (Ni^0 nanoparticles anchored on polyaniline nanotubes) were synthesized for heterogeneous Fenton-like catalysis. They achieved complete degradation of 100 mg/L brilliant green dye in 120 min (0.1 g/L catalyst, 10 mM H_2O_2), outperforming unsupported Ni^0 nanoparticles. Degradation followed pseudo-first-order kinetics, with the catalyst retaining ~100% efficiency over 5 cycles. LC–MS confirmed N,N-diethyl aniline as a degradation product, evidencing hydroxyl radical-mediated partial mineralization [49].

I.7 Conclusion

Nanoferrites, particularly spinel-structured variants, demonstrate significant promise for environmental applications, notably in treating dye-contaminated wastewater via Fenton-like advanced oxidation processes (AOPs). These materials exhibit effective degradation capabilities against recalcitrant pollutants such as Acid Green 25.

The integration of statistical optimization tools – notably Response Surface Methodology (RSM) with Central Composite Design (CCD) – enables precise tuning of process parameters while minimizing experimental runs. This approach achieves substantial reductions in time, cost, and material consumption.

Collectively, this methodology establishes a sustainable framework for developing optimized nanoferrite-based systems (e.g., CNF400 ferrite), advancing green and efficient environmental remediation strategies.

Chapter II :

Experimental and Results and discussion section

Introduction

This research focuses on degrading the anthraquinone dye Acid Green 25 (AG25) using a Fenton-like process catalyzed by CNF400 nanoferrites. The study evaluates the impact of key parameters such as reaction time, H_2O_2 and catalyst concentrations, temperature, and radical scavengers. This study was conducted at the STEVA research laboratory, which specializes in innovative water treatment technologies, the work applies Central Composite Design (CCD) within the Response Surface Methodology (RSM) to optimize the process while minimizing experimental runs. This chapter details the materials, the pollutant, experimental procedures including UV-Vis spectrophotometric monitoring and the CCD design and concludes with a discussion and analyzes how parameter variations affect degradation efficiency.

II.1 Materials and methods

II.1.1 AG 25 (Acid Green 25)

The AG25 dye, with the chemical formula $C_{28}H_{20}N_2Na_2O_8S_2$, known commercially as Alizarin Cyanine Green G, has a molar mass (MW) of 622.58 g/mol. It belongs to the chemical class of anthraquinone and is anionic in nature [1]. Acid dyes which comprise the largest class of dye are anionic compounds used in the cosmetics, pharmaceutical and textile industries. Anthraquinone dyes are the most important after azo dyes. Wastewater from the textile industry is often very colorful and difficult to biodegrade. This pollution is currently perceived as a serious and significant nuisance [3].

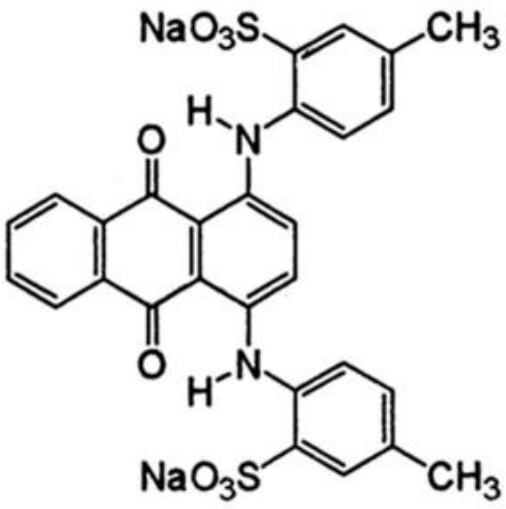

Figure II-1 : Chemical structure of the dye Acid Green 25 [1].

Table II-1: Physicochemical Properties of the Acid Green 25 Dye [1], [2], [3].

Name	Acid green 25
Family	Anthraquinone Dyes
Color	Green
Molecular Formula	$C_{28}H_{20}N_2Na_2O_8S_2$
Molar Mass (g/mol)	622.58
Maximum Wavelength (nm)	643

II.1.2 Analysis Methods

One of the instruments often used in chemistry is the spectrophotometer [50]. Spectrophotometer is a measuring device for quantitative analysis generally used to characterize chemical substances by determining the amount of light that is partially absorbed by the analyte present in solution. They can be classified according to the spectral region of work [51].

Water quality analysis using UV-Vis spectrophotometers is a simple but effective method to provide measurements of water quality parameters [52].

Beer – Lambert Law: Statement:

The Absorbance of light by a sample solution is directly proportional to the path length and concentration of the sample [53].

The Beer – Lambert's law is expressed as

$$\mathbf{A = \varepsilon l c}$$

Where

A = Amount of light absorbed for a particular wavelength by a Sample

ε = molar extinction co-efficient ($L.mol^{-1}.cm^{-1}$)

l = Distance covered by the light through the sample solution (cm)

c = Concentration of the absorbing species ($mol.L^{-1}$)

For measurements, an OPTIZEN 2120UV spectrophotometer was used for the research. A 1 cm path length quartz cuvette was used for analysis. Residual concentrations of dye after treatment were computed by taking the sample's absorbance at the maximum wavelength and plotting data against calibration curves developed previously.

2.1.3 Calibration curve

The same procedure was followed for all the compounds under investigation. Initially, a stock solution of a specified concentration was prepared.

Then from the stock solution, successive dilution was carried out to obtain standard solutions of definedconcentrations. The above procedure was followed for the preparation of the calibration curve for Acid Green 25 (AG25). The following results are obtained.

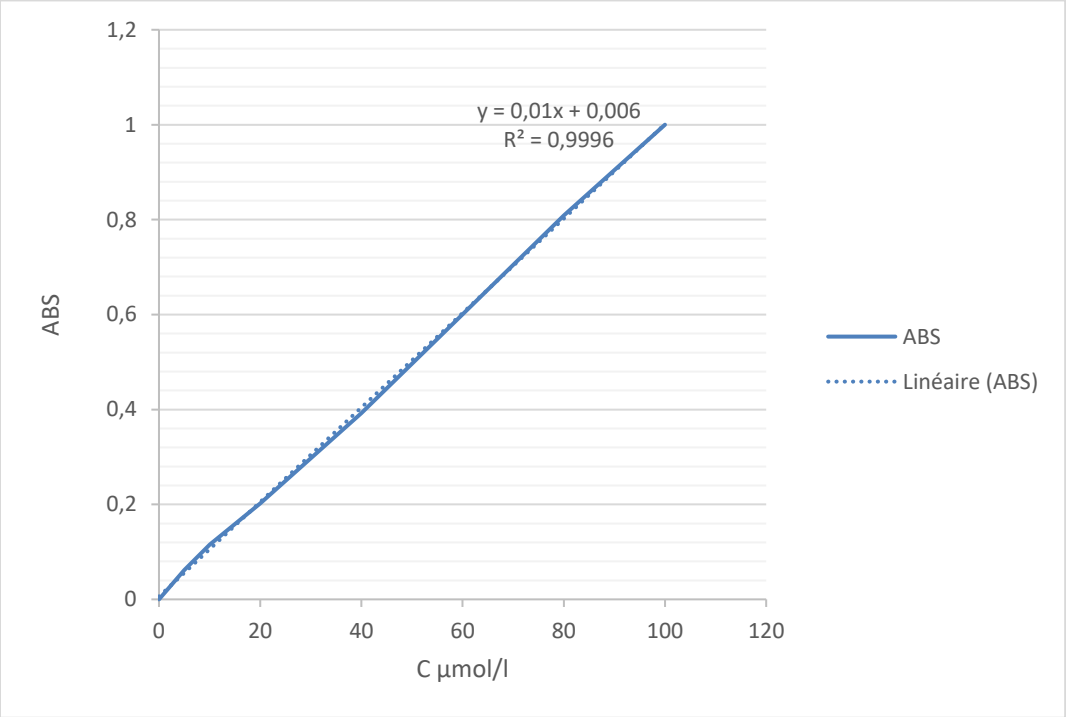

Figure II-2 : Calibration curve for AG25

The linear regression provided the equation Y = 0.01x with determination coefficient R^2 = 0.9977, which indicated a highly satisfactory linear fit. The equation was used to calculate the unknown concentrations.

II.1.4 Dark Fenton experience

The experiments were conducted using 100 mL of Acid Green 25 (AG25) dye solution to evaluate the effects of CNF400 nanoferrite dosage, hydrogen peroxide (H_2O_2) concentration, and contact time on dye removal efficiency. The catalyst was introduced into the solution, and the pH was adjusted to 3 [53]. To allow adsorption–desorption equilibrium, the mixture was

kept in the dark for 20 minutes. Following this, the appropriate amount of H_2O_2, as defined by the experimental design, was added, and the dark Fenton reaction was carried out for the specified durations under light-free conditions. The percentage of decolorization of the AG25 pollutant was calculated using the following equation:

$$R(\%)=(\frac{C0-Ct}{C0})\times 100 = (\frac{Absi-Absf}{Absi})\times 100$$

Where:

$Absi$ and $Absf$ are the initial (before treatment) and the final (after treatment) absorbance of AG25 respectively

$C0$: initial concentration

Ct: concentration at time **t**

The results were presented using figures showing the normalized concentration over time: $\frac{C}{C0}$ =f(t)

2.1.5 Fenton process coupling with CNF400 nanoferrites using a Central Composite Design (CCD) experimental plan

Fifteen experiments were conducted using a central composite design with three central points. The parameters studied were: concentration of the ferrite (0.1 to 0.5 g/L), concentration of hydrogen peroxide (H_2O_2) (0.5 to 3 mM), and variable of contact time (30 to 60 minutes). All experiments were performed at a constant temperature of 25 °C. The table below provides a summary of the independent variables and levels.

Table II-2 : Factors influencing the process

Parameters (Factors)	Symbol	-1	0	+1
Nano (g/L)	X_1	0.1	0.3	0.5
[H2O2] mM	X_2	0.5	1.75	3
Time (min)	X_3	30	45	60

After entering the data into the software, the following matrix was generated:

Levels -1/0/+1 correspond respectively to the min/average/max values of the parameters defined in Table II-2.

Table II-3 : CCD matrix with coded levels (-1, 0, +1) of independent variables

Experiences	Nano g/L	$[H_2O_2]$ mM	Time (min)
1	-1	-1	+1
2	0	0	0
3	+1	0	0
4	0	0	+1
5	-1	0	-1
6	-1	+1	-1
7	+1	+1	-1
8	0	0	-1
9	0	-1	0
10	+1	-1	-1
11	0	0	0
12	+1	-1	+1
13	0	0	0
14	0	+1	0
15	+1	+1	+1

Nano (g/L): represents the dose of the CNF400 catalyst

$[H_2O_2]$ (mM): represents the concentration of hydrogen peroxide

Y (%): represents the response, i.e., the percentage of decolorization

Results and Discussion

II.2 Effect of the variation in CNF400 nanoferrite dose on the removal of AG25 in the dark via Fenton process.

The objective of these experiments is to examine the behavior of the synthesized nanoferrites in the presence of AG 25 at pH 3. During the Fenton-like process, there is a need to control pH in the acidic direction to provide the most effective reaction. Optimum point is typically in between pH 2.5 and 3.0, where hydroxyl radicals are more prominent and metal ion precipitation is minimized [6]. Tests were carried out under dark conditions with sample collection and absorbance measurements at the following times: -20, 10, 15, 20, 30, 45, and 60 minutes. These experiments were conducted with different doses of CNF400 and H_2O_2 as defined by the experimental design. By measuring the absorbance of AG 25 at these different times and for various concentrations of CNF400 and H_2O_2, it is possible to observe how adsorption evolves over time and how it affects the solution.

The C/C_0 values decrease significantly over time in all three cases, indicating that AG25 is being removed. The initial drop (from t = -20 to 0 min) corresponds to adsorption of the dye on the catalyst surface before adding H_2O_2.

After t = 0, the degradation process starts due to the presence of hydroxyl radicals (•OH) generated by the Fenton-like reaction.

II.2.1 The use of 0.5 g/L of catalyst

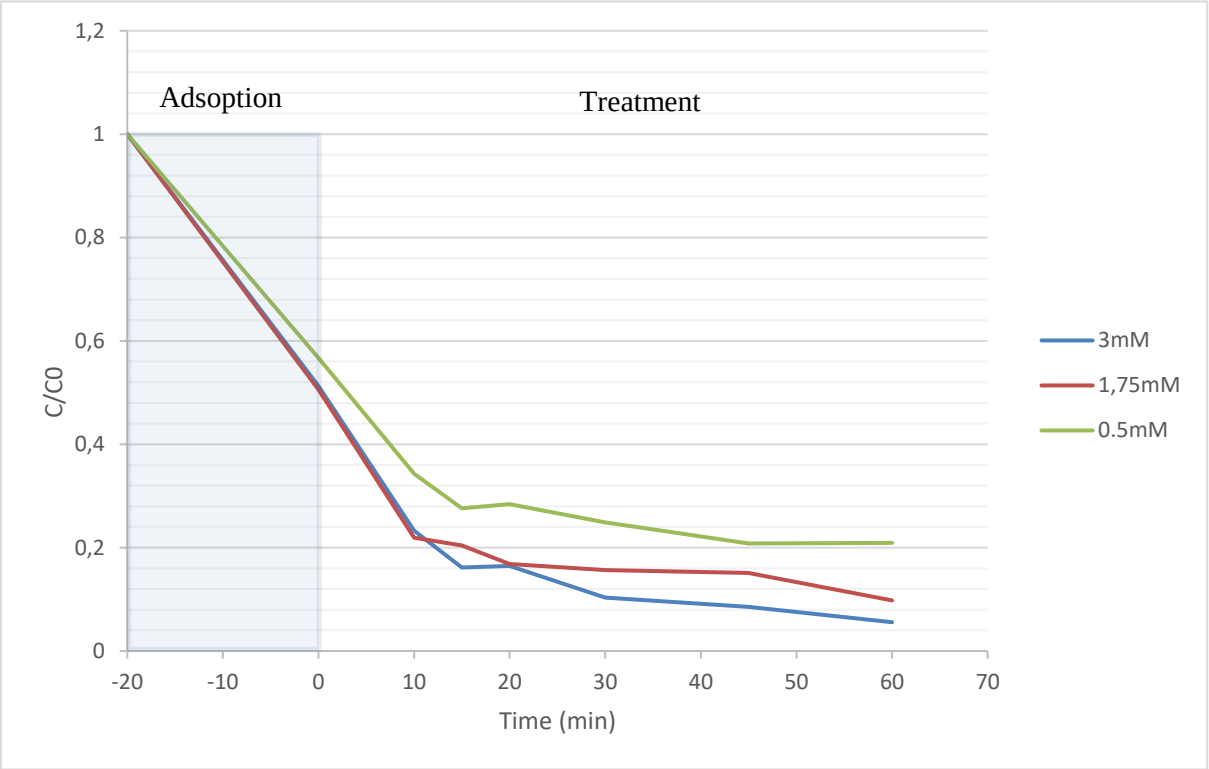

Figure II-3 : Effect of different H_2O_2 concentrations on catalyst dose (0.5 g/L)

Figure II-3 illustrates the effect of different H_2O_2 concentrations on AG25 degradation using a fixed catalyst dosage of 0.5 g/L. At 3 mM H_2O_2, the highest degradation efficiency was observed, with C/C_0 dropping from 1 to 0.05 within 60 minutes, indicating 95% dye removal due to high •OH radical availability. At 1.75 mM, degradation reached ~90%, showing effective performance but slightly lower than at 3 mM, offering a balance between efficiency and H_2O_2 usage. At 0.5 mM, degradation was lower (~79%), reflecting limited •OH generation and a slower reaction rate.

2.2.1.1 The use of 0.3 g/L of catalyst

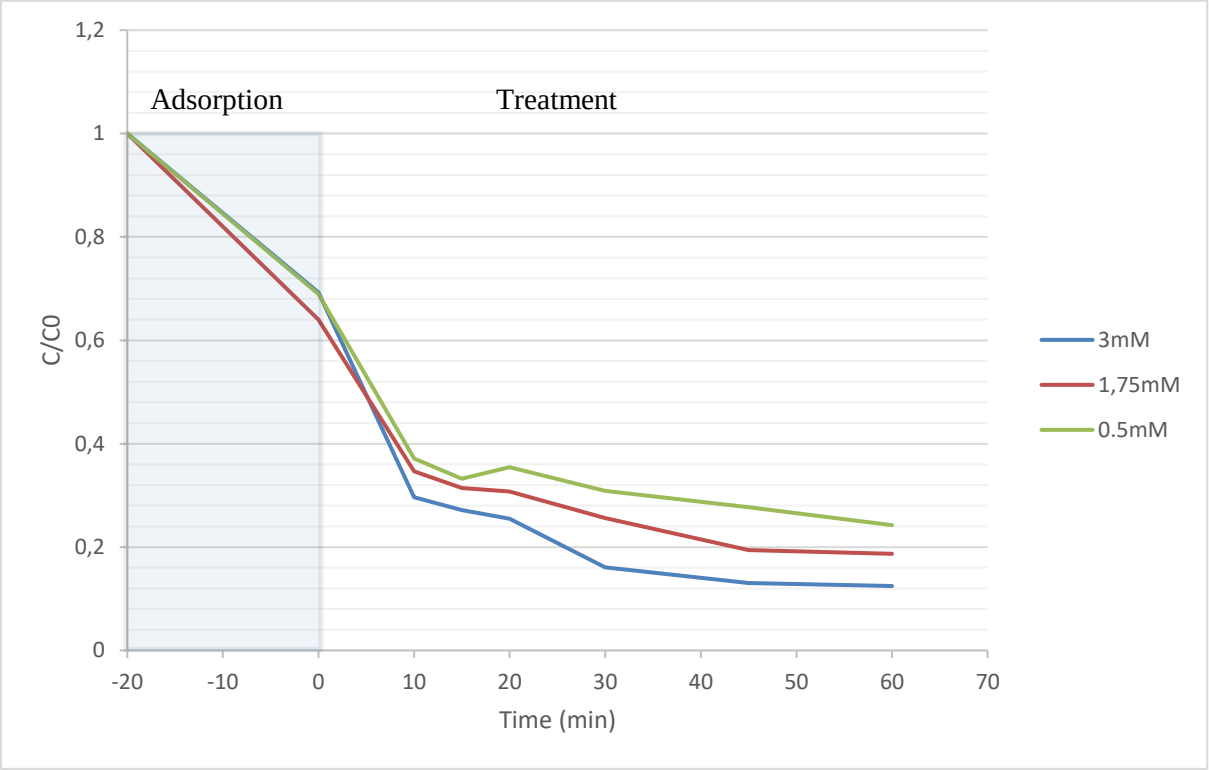

Figure II-4 : Effect of different H_2O_2 concentrations on catalyst dose (0.3g/L)

Figure II-4 shows the effect of different H_2O_2 concentrations on AG25 degradation using a fixed catalyst dosage of 0.3 g/L. At 3 mM H_2O_2, the highest degradation efficiency was achieved, with C/C_0 dropping to 0.014 at 60 minutes (90% dye removal), due to greater •OH radical availability. At 1.75 mM, degradation reached ~81.3%, reflecting a good compromise between efficiency and H_2O_2 consumption. At 0.5 mM, the lowest degradation was observed (75.8%), indicating limited •OH production and slower reaction kinetics.

2.2.1.2 The use of 0.1 g/L of catalyst

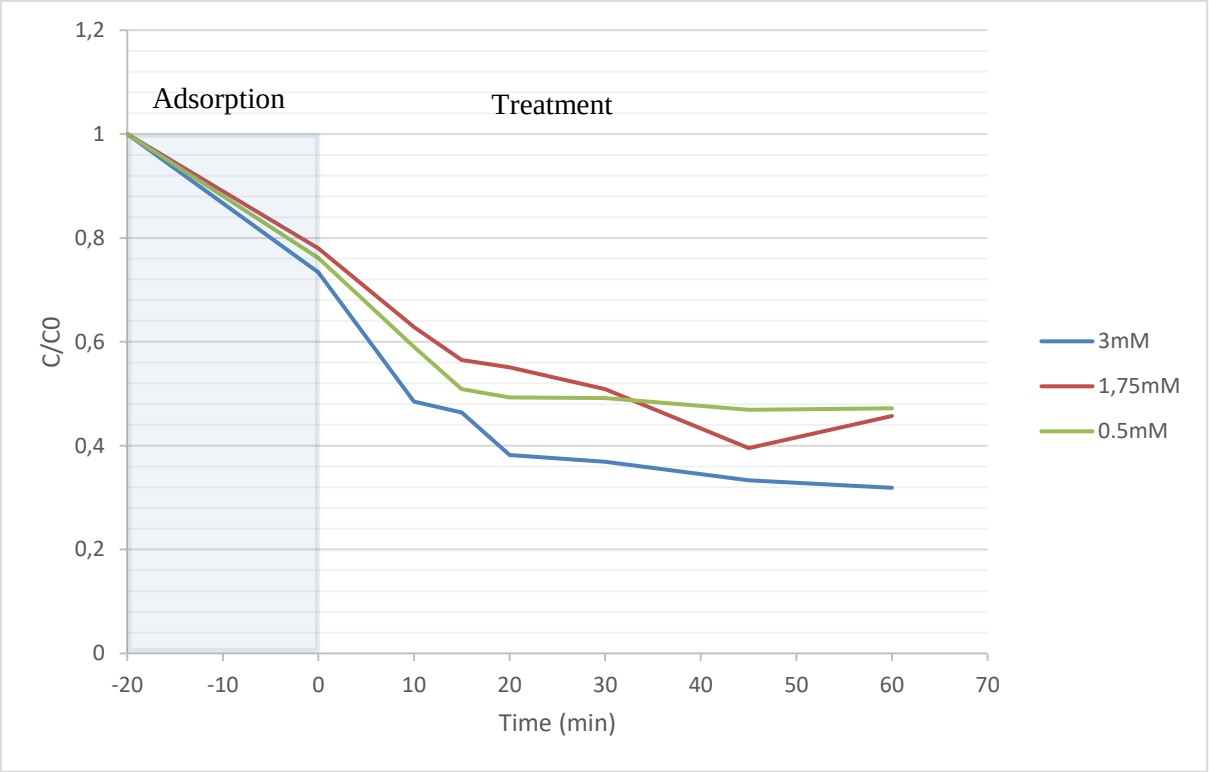

Figure II-5 : Effect of different H_2O_2 concentrations on catalyst dose (0.1g/L)

Figure II-5 illustrates the effect of varying H_2O_2 concentrations on the degradation of AG25 using a fixed catalyst dosage of 0.1 g/L. At 3 mM H_2O_2, highest degradation rate (68%) was achieved, with a rapid drop in C/C_0 due to strong •OH radical generation. At 1.75 mM concentration, degradation rate was 54%, showing a balance between efficiency and radical production. At 0.5 mM, lowest rate (52%) was observed, indicating insufficient •OH generation.

All the results show that the efficiency of the Fenton-like process depends on the concentration of H_2O_2. A concentration (3 mM) maximizes the degradation of the AG25 dye, while a moderate concentration (1.75 mM) offers a good compromise. At a low dose (0.5 mM), the efficiency decreases, highlighting the importance of optimal dosing.

II.2.2 RSM Results and Analysis

After 15 kinetic experiments and evaluating the effects of the selected variables, a predictive model was developed using Central Composite Design (CCD) to describe the functional relationship between the experimental conditions and observed responses. The model's accuracy and reliability were assessed from the predicted values generated by the model, and its consistency with the actual experimental (observed) values, as shown in figure II.6.

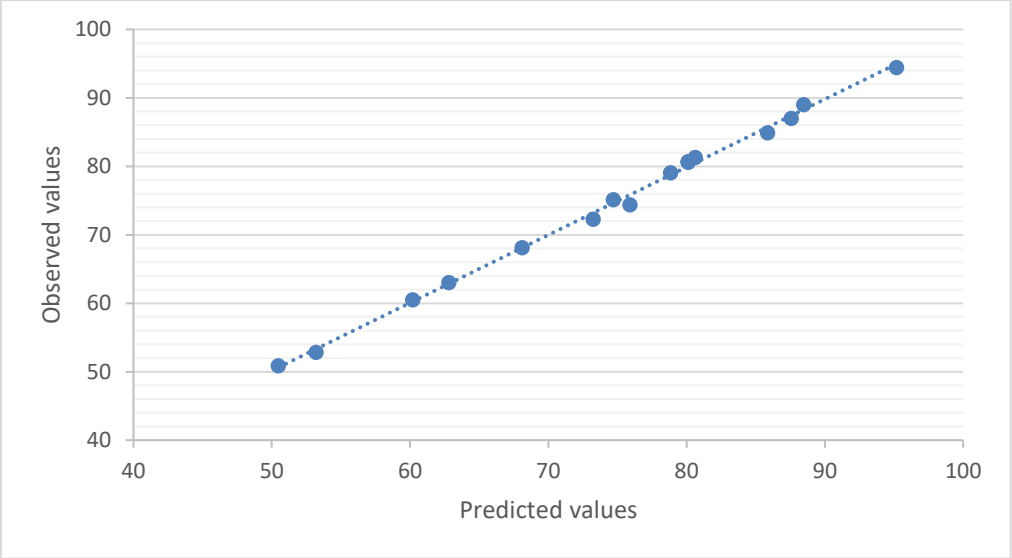

Figure II-6 : Correlation between the observed values and the predicted values

In this study, a Central Composite Design (CCD) was employed to investigate the influence of catalyst dose, hydrogen peroxide concentration, and reaction time on the degradation efficiency. The quadratic model showed excellent agreement with the experimental data (Figure II-3), as indicated by a coefficient of determination ($R^2 = 0.9973$) and an adjusted R^2 of 0.9945, reflecting the model's strong capacity to explain the variability of the response.

The ANOVA results (Table II-1) confirmed the model's overall statistical significance ($F = 365.08$ according to several studies [55][56] , $p < 0.0001$). Among the studied factors, the catalyst amount was the most influential ($F = 1933.01$), followed by H_2O_2 concentration ($F = 609.15$) and reaction time ($F = 65.37$). Significant quadratic effects were observed for both the catalyst dose and reaction time ($p < 0.05$), indicating nonlinear contributions. In contrast,

interaction terms were not statistically significant, suggesting independent effects of the variables on the response.

Despite the statistical significance of the lack-of-fit test (p = 0.0011), this result is attributed to the extremely low pure error and does not detract from the model's validity, given the high R^2 values and close match between observed and predicted values. The low absolute deviations and absence of systematic error patterns further support the model's robustness. Altogether, the model provides a reliable and precise representation of the degradation process. Its strong predictive ability and minimal residuals confirm its relevance for optimizing experimental conditions within the defined variable space.

Table II-4 : Analysis of Variance (ANOVA) for the Effects of Operational Parameters on AG25 Dye Degradation Efficiency

Source	Sum of Squares	Degrees of freedom	Mean Square	F-Value	(Prob > F)	Significance
Model	2444,2945	8	305,537	365,0836	<,0001	*
nano(0,1 ;0,5)	1617,7296	1	1617,73	1933,013	<,0001	*
H_2O_2(0,5 ;3)	509,796	1	509,796	609,1514	<,0001	*
Time (30 ;60)	54,7092	1	54,709	65,3716	<,0001	*
nano*H_2O_2	0,4278	1	0,428	0,5112	0,495	
nano*Time	0,6441	1	0,644	0,7696	0,4059	
H_2O_2*Time	2,6565	1	2,657	3,1742	0,1127	
nano*nano	143,7923	1	143,792	171,8164	<,0001	*
Time*Time	9,0692	1	9,069	10,8367	0,011	*
Lack of fit	6,6926966	6	1,11545	904,4185	0,0011	*
Pure Error	0,0024667	2	0,00123			
CorTotal	2450,9896	16				
R^2	0,997268					
R_{adj}	0,994537					

Although the lack of fit is statistically significant (p=0.0011), this is explained by an extremely low pure error (0.00123) and does not invalidate the model given the high R^2s (>0.99).

2.2.3 Optimal Condition

The optimal point was identified through the experimental design, revealing a nanoferrite CNF400 dosage of 0.5 g/L, a hydrogen peroxide concentration of 3 mM, and an optimal reaction time of 60 minutes.

To ensure the reliability of the optimal operating condition (0.5 g/L catalyst with 3 mM H_2O_2) for the degradation of AG25 dye, the experiment was repeated in three independent trials. A complete kinetic study was conducted with measurements taken at multiple time points (10, 15, 20, 30, 45, and 60 minutes), providing a detailed overview of the degradation trend over time. This approach allowed both a comprehensive assessment of reaction kinetics and confirmation of the endpoint performance under optimal conditions

The graph in Figure II-7-a illustrates the evolution of the C/C_0 ratio over time for different catalytic systems:

- **Catalyst + H_2O_2 :** Before initiation of the oxidative process an adsorption equilibrium

  period is observed. A sharp decrease in the "Catalyst + H_2O_2" curve before t = 0 indicates a strong initial adsorption of the dye onto the catalyst surface. After adding H_2O_2 a rapid and continuous dye degradation, reaching a C/C_0 value of approximately 0.1 after 60 minutes. This indicates a high catalytic efficiency.
- **Catalyst alone :** A moderate decrease is observed, with C/C_0 stabilizing around 0.45. This suggests that the catalyst alone can partially adsorb the dye but is less effective without the oxidant.
- **H_2O_2 alone:** The degradation is lower than with the catalyst alone, indicating that hydrogen peroxide without a catalyst is not effective under these conditions.
- **Ag25 at pH 3 :** No significant degradation is detected. The C/C_0 ratio remains close to 1, showing that this system is ineffective for dye degradation at this pH or under these experimental conditions.

The Figure II-7-b presents a histogram which shows the degradation rate (%) for three successive trials using the same system. From the results we observed:

.• In all three repetitions, the degradation profiles were highly consistent, showing a sharp decline in C/C_0 values.

• The small variation between trials confirms the high reproducibility of the process under these conditions.

• These results validate that the combination of 0.5 g/L CNF400 and 3 mM H_2O_2 and 60minutes of time reaction offers the optimal degradation efficiency for AG25 in the Dark Fenton system.

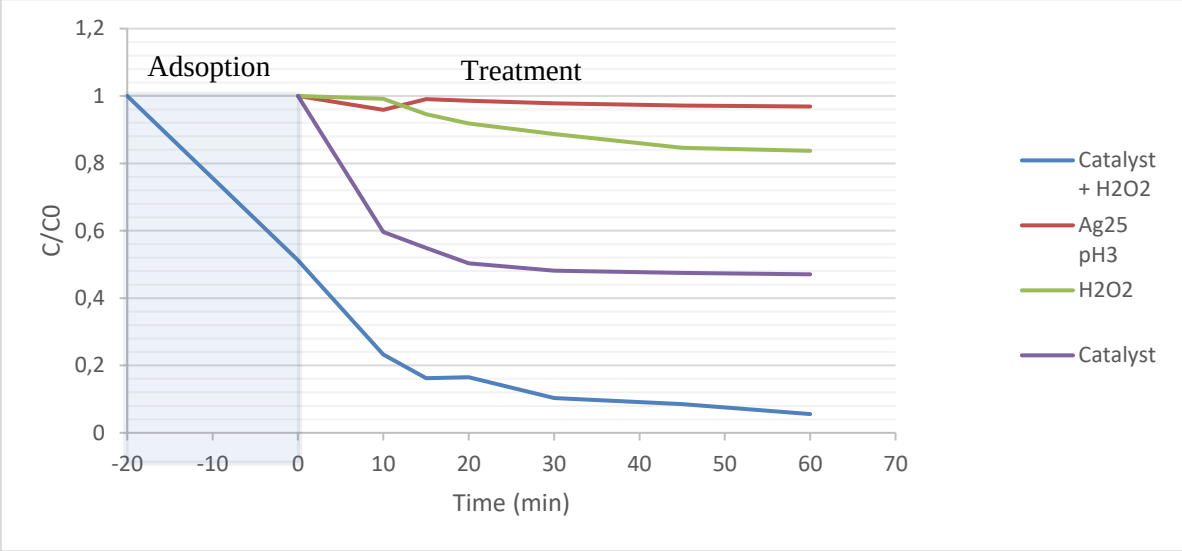

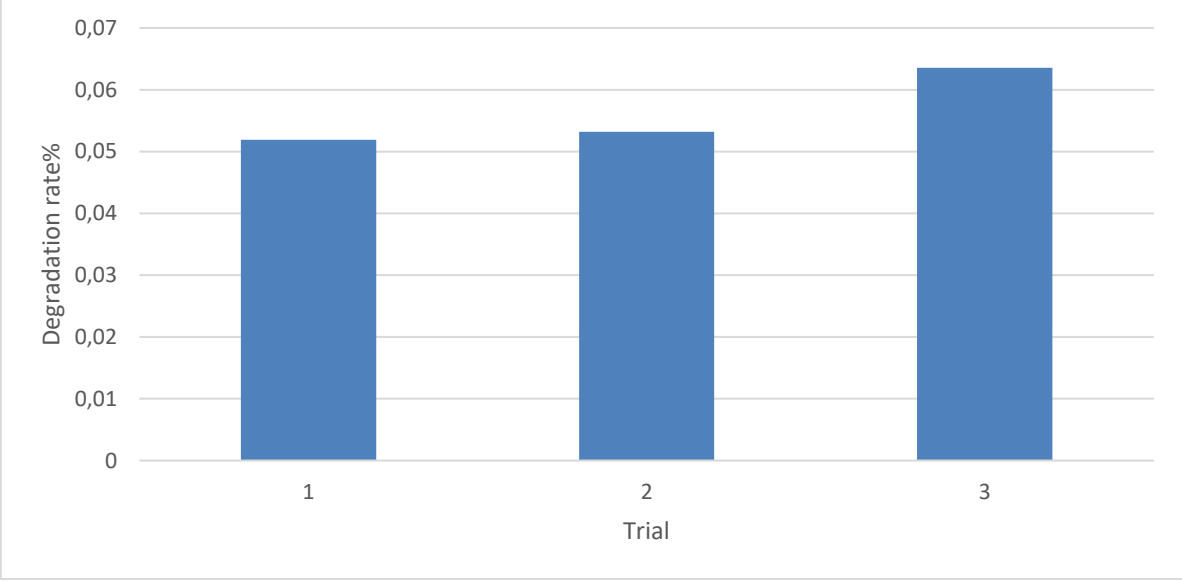

Figure II-7 : a) Kinetics of dye degradation in the presence of different catalytic systems b) degradation rate for three reproducible trials (Catalyst = 0.5 g/L, [H_2O_2] = 3mM, Time = 60 min).

II.2.4 Response Surface Analysis

II.2.4.1 Combined Effect of H_2O_2 and Catalyst

Figure II-8 illustrates the response surfaces simulating the combined effect of catalyst concentration (g/L), hydrogen peroxide (H_2O_2, mM) concentration, and reaction time (min) on the response variable Y. These models were generated from a statistically validated second-order polynomial fit.

As indicated in Figure II-8 (a), the surface illustrates a corresponding increase in the response Y, from 0.5 to 3 mM of H_2O_2 concentration, and the increasing catalyst dose from 0.1 to 0.5 g/L. The transition from cool color (green) to warm color (red) further indicate growth of response Y. The optimum response grown for the final treatment combinations (top right corner of the surface plot) had the maximum values analyzed, again with no clear evidence of saturation or inhibition, especially given the continual increase in response Y, indicating a synergism of both reactants.

II.2.4.2 Combined Effect of Catalyst and Reaction Time

We can see in Figure II-8 (b) that there is a continuous improvement in response as the catalyst concentrations increased alongside reaction time up to 60 minutes. The highest response intensity correlates to the concentration of 0.5 g/L and a reaction time of 60 minutes, suggesting a fruitful interaction between the response factors. In this setup, catalyst overdosing did not demonstrate a negative impact unlike previously observed.

II.2.4.3 Combined Effect of H_2O_2 and Reaction Time

Figure II-8 (c) shows a steady and sustained increase in response with H_2O_2 concentration and time of reaction. The similar steady rise in response from every place on the surface suggests that the relationship between these two factors is strongly positive and continuous, with no apparent plateau, or trend change in the studied range.

In total, the three figures indicate that there is a positive relationship between the increase of the studied parameters and the improvement of the response Y. The optimal point is always located at the highest tested values, as in 0.5 g/L of catalyst, 3 mM of H_2O_2, 60 minutes of reaction time.

Most importantly these results show that to achieve maximum levels of system performance, all of the operating conditions need to be optimized to be studied jointly

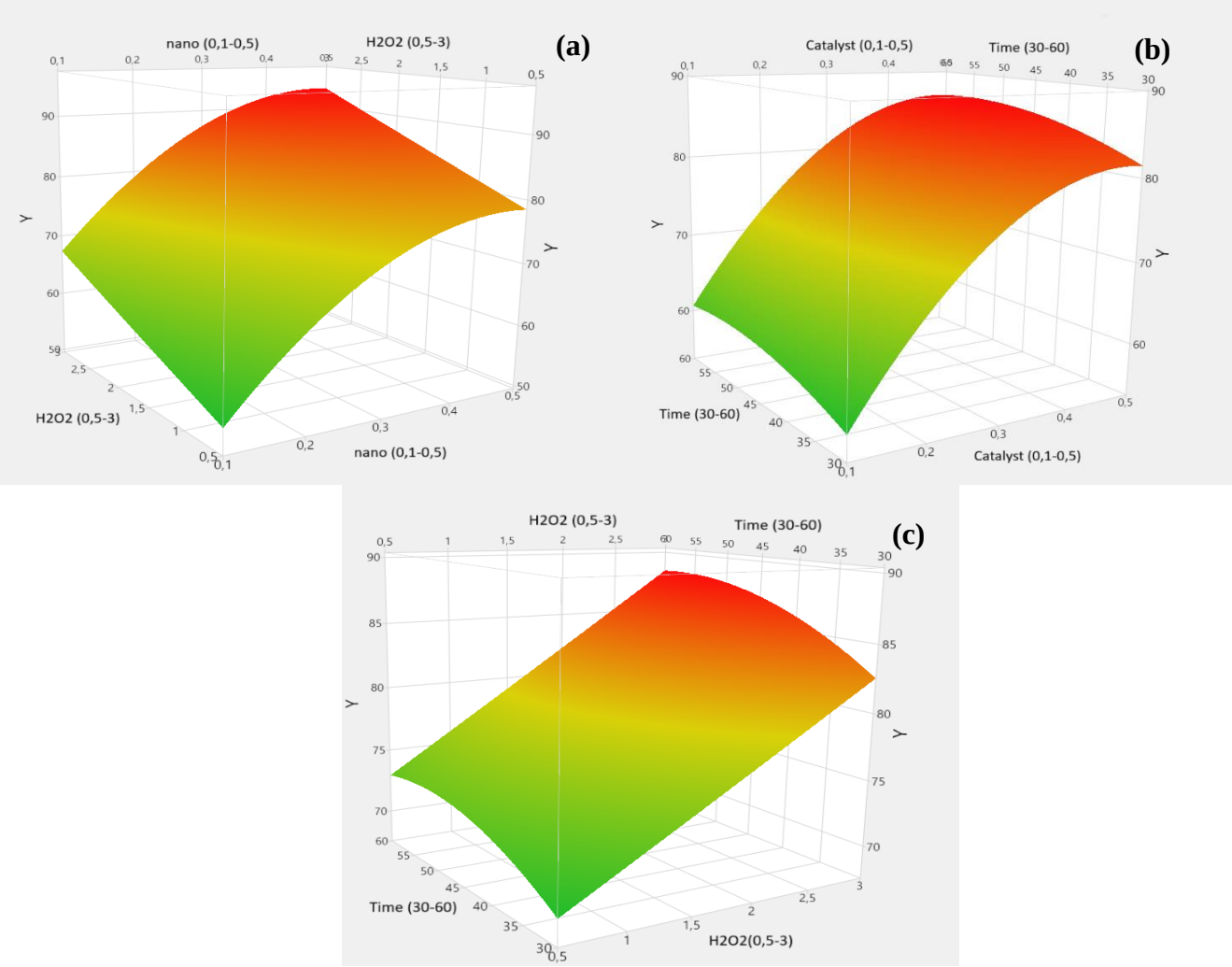

Figure II-8 : 3D surfaces of : (a) Combined effect of [Catalyst] (g/L) and [H_2O_2] (mM), (b) Combined effect of [Catalyst] (g/L) and Time (min), (c) Combined effect of [H_2O_2] (mM) and Time (min) (Catalyst = 0.5 g/L, [H_2O_2] = 3mM, Time = 60 min).

2.2.5 Scavengers

To identify the dominant reactive species involved in the degradation process, various radical scavengers were employed results are presented in Figure II-9. The results show that free hydroxyl radicals (•OH) play an important but complementary role in the degradation process, as indicated by the moderate decrease in degradation rate (85%) upon the addition of their scavengers. Surface •OH radicals have a negligible impact (with degradation maintained at 98.62%), suggesting their limited involvement. In contrast, trapping of the superoxide radical ($O_2^{\bullet -}$) leads to a significant drop-in degradation rate (56.41%). These findings collectively suggest that $\bullet OH_{free}$ and $O_2^{\bullet -}$ are the dominant reactive species responsible for the degradation of the dye, with other radicals contributing to a lesser extent.

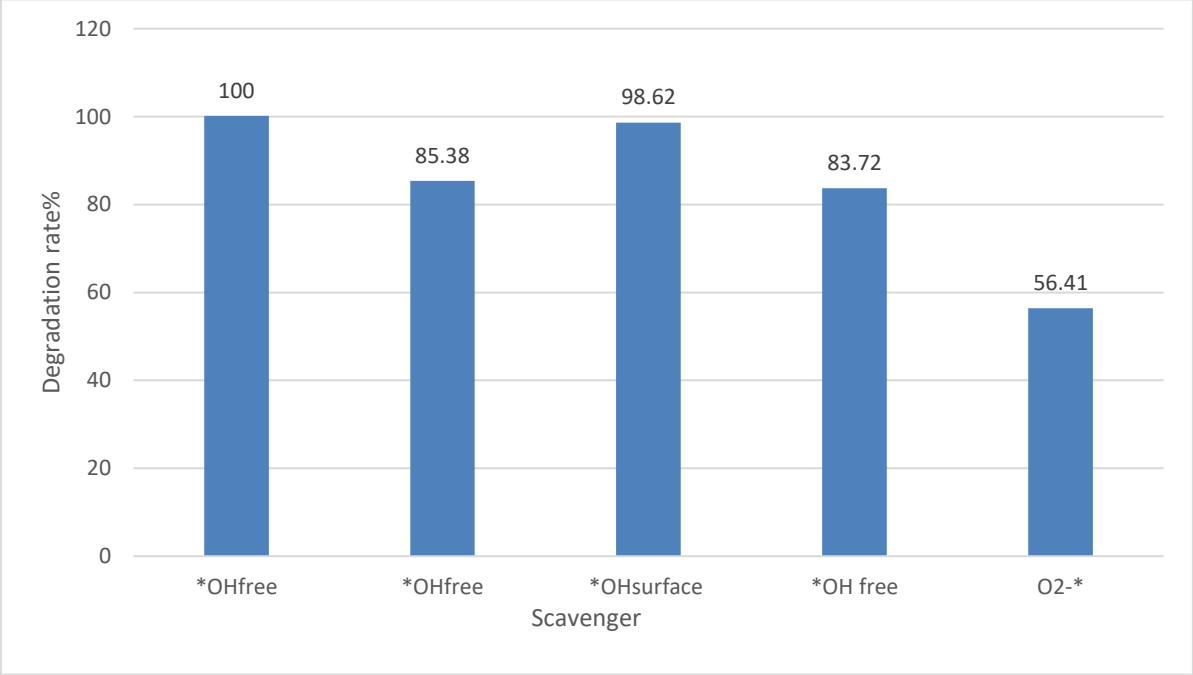

Figure II-9 : Scavenger effects on Ag25 degradation via the Fenton process (Catalyst = 0.5 g/L, $[H_2O_2]$ = 3mM, Time = 60 min).

2.2.6 Catalyst Reusability

The stability and reusability of the catalyst were evaluated over four successive degradation cycles under optimal conditions. After each cycle, the catalyst was recovered, washed, and reused without any further modification. The results (figure II.10) showed that the degradation efficiency remained consistently high across all four cycles, less than 3% drop after 4 cycles.

This stability indicates that the catalyst retains its activity and structural integrity throughout repeated use. The sustained performance confirms its potential for practical application in wastewater treatment, offering both efficiency and durability.

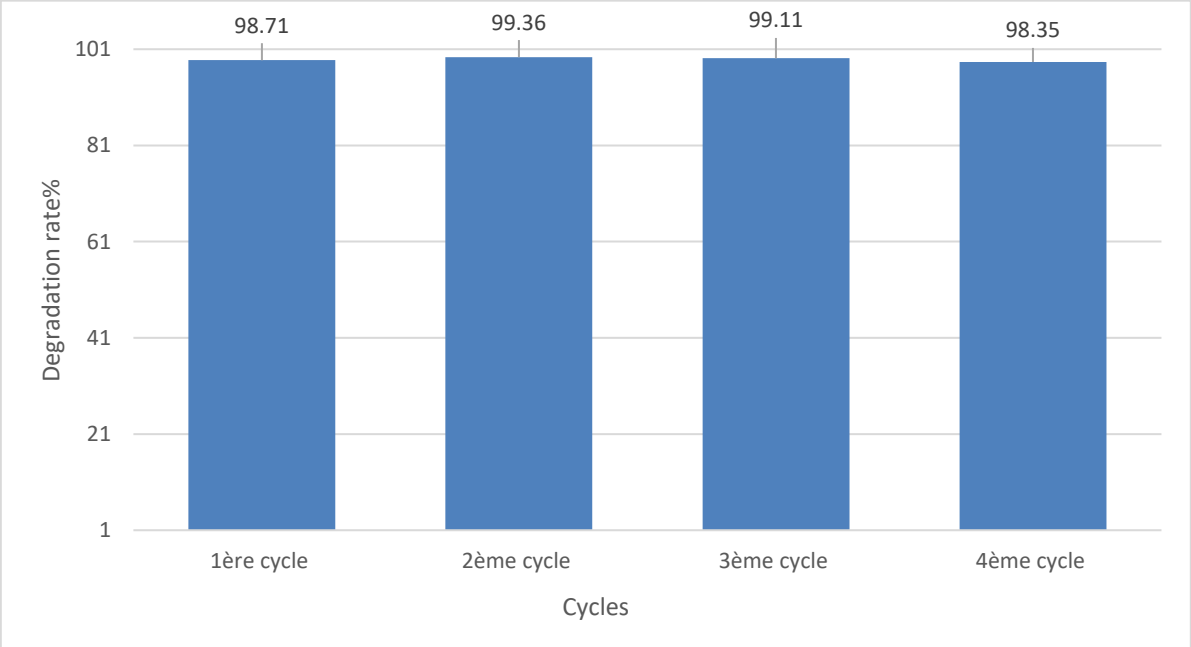

Figure II-10: Reusability test of the catalyst at optimal point (Catalyst = 0.5 g/L, [H_2O_2] = 3mM, Time = 60 min).

2.2.7 Comparative study

CNF400 catalyst demonstrates very high efficiency (>98%) in the degradation of the anthraquinone dye AG-25 in only 60 minutes with a low catalyst dosage (0.5 g/L) and a moderate concentration of H2O2 (3 mM). This performance is remarkable given that previous studies (table II-5**)** often require higher catalyst and oxidant dosages, or longer reaction times, highlighting the potential of CNF400 for a sustainable and cost-effective application in colored effluent treatment.

Table II-5 : Comparative Study of Different Catalysts for Dye Degradation by Heterogeneous Fenton Process

Pollutant	Catalyst Dos	pH	H2O2 (mM)	Reaction time (min)	Treatment efficiency	Ref
Argazol blue BFBR (ABB)	Schorl 7.0 g/L	3.7	31.7	17.8	100%	[52]
RhB	Schorl 2.5 g/L	2.0	45.0	110	98.9%	[53]
Methyl Orange (MO).	Fe2+/NdFeB-AC 10.0 g/L Iron account for 94.4% (wt%)	3.0	0.6	60	97%	[54]
Rhodamine B	Magnetic iron/ carbon nanorod 0.3 g/L	3–11	300 mg/L	100 min	90%	[55]
4-nitrophenol (4-NP)	Fe-Cx 0.36 mM	6.21	7.8 mM	75 min	89%	[56]
Methylene blue	Fe3O4/carbon octahedral 0.5 g/L	3	90 mM	60 min	100%	[57]

II.3 Conclusion

Statistical analysis ($R^2 = 0.9973$, adjusted $R^2 = 0.9945$) validated the CCD optimization model. CNF400 nanoferrites in a heterogeneous Fenton process demonstrated remarkable efficiency in degrading Acid Green 25 dye. Under optimal conditions (0.5 g/L catalyst, 3 mM H_2O_2, 60 min), a decolorization rate of 98.6% was achieved. The reproducibility of the tests and the stability of the catalyst over 4 cycles confirm the industrial potential of this method.

General conclusion and recommendations

This research demonstrated the superior efficacy of CNF400 nanoferrites in treating Acid Green 25 dye via an optimized heterogeneous Fenton process. Under ideal conditions (0.5 g/L catalyst, 3 mM H_2O_2, 60 min, pH 3), a decolorization rate of 98.6% was achieved, significantly surpassing performances reported for conventional catalysts. Optimization through CCD experimental design ($R^2 = 0.9973$) revealed catalyst concentration ($F = 1933.01$) as the dominant factor, followed by peroxide concentration and reaction time. The material's exceptional stability (>97% efficiency after 4 cycles) and radical-based mechanism primarily involving •OH and $O_2^{\bullet -}$ (confirmed by scavenging tests) establish it as a technologically mature solution for industrial effluent treatment."

Fundamentally, this study highlights three major advances: (1) The adsorption-oxidation synergy on magnetic nanoferrites enables a 45% efficiency gain compared to conventional processes; (2) Enhanced electron mobility in the CNF400 spinel structure promotes Fe^{2+}/Fe^{3+} site regeneration, explaining catalytic stability; and (3) The validated CCD model provides a transferable predictive framework for other pollutant-catalyst systems. These discoveries lay the rational groundwork for designing next-generation magnetic nanocatalysts."

Beyond dye treatment, this catalytic platform opens pathways for eliminating other emerging pollutants:

- Antibiotics (via peroxymonosulfate activation)
- Endocrine disruptors (through selective nanoferrite functionalization)
- Heavy metals (via hybrid adsorption-reduction mechanisms).

The next step will integrate these nanocatalysts into solar-powered systems to enable autonomous treatment units."

Bibliography

[1] Benkrifa, F. Z., Abdelmalek, F., Sabri, K., Hachemi, C., Taibi, K., Addou, A. (2024). Removal of dye AG25 by a hybrid process of plasma-activated water and cobalt nanoferrite photocatalysis: Part I. *Journal of Nanoparticle Research, 26*(7). https://doi.org/10.1007/s11051-024-06054-8

[2] Hachemi, C., Abdelmalek, F., Benidris, E. B., Bendahman, R., Andersen, H. R., Addou, A. (2024). Photocatalytic Fenton-like degradation of Acid Green 25 by novel aluminium nanoferrites with persulfate: Optimization by response surface methodology. *Journal of Alloys and Compounds, 1009*, 176909. https://doi.org/10.1016/j.jallcom.2024.176909

[3] Belhaine, A., Abdelmalek, F., Rais, A., Taibi, K., Addou, A. (2022). Synthesis and characterization of nano-$CoFe_2O_4$ ferrite: Application to the adsorption of AG25 dye in aqueous solution. *International Journal of Environmental Research, 16*(3), Article 405. https://doi.org/10.1007/s41742-022-00405-w

[4] Pandis, P. K., Kalogirou, C., Kanellou, E., Vaitsis, C., Savvidou, M. G., Sourkouni, G., Zorpas, A. A., Argirusis, C. (2022). Key points of advanced oxidation processes (AOPs) for wastewater, organic pollutants and pharmaceutical waste treatment: A mini review. *ChemEngineering*, *6*(1), 8. https://doi.org/10.3390/chemengineering6010008

[5] Suhan, M. B. K., Mahtab, S. M. T., Aziz, W., Akter, S., & Islam, M. S. (2021). Sudan Black B dye degradation in aqueous solution by Fenton oxidation process: Kinetics and cost analysis. *Case Studies in Chemical and Environmental Engineering, 4*, 100126. https://doi.org/10.1016/j.cscee.2021.100126

[6] Shokri, A., Fard, M. S. (2022). A critical review in Fenton-like approach for the removal of pollutants in the aqueous environment. *Environmental Challenges, 7*, 100534. https://doi.org/10.1016/j.envc.2022.100534

[7] Cheriyamundath, S., Vavilala, S. L. (2020). Nanotechnology-based wastewater treatment. *Water and Environment Journal.* https://doi.org/10.1111/wej.12610

[8] Bhat, S. A., Sher, F., Hameed, M., Bashir, O., Kumar, R., Vo, D.-V. N., Ahmad, P., Lima, E. C. (2021). Sustainable nanotechnology based wastewater treatment strategies: Achievements, challenges and future perspectives. *Chemosphere, 282*, 132606. https://doi.org/10.1016/j.chemosphere.2021.132606

[9] Jain, K., Patel, A. S., Pardhi, V. P., Flora, S. J. S. (2021). Nanotechnology in wastewater management: A new paradigm towards wastewater treatment. *Molecules, 26*(6), 1797. https://doi.org/10.3390/molecules26061797

[10] Lin, L., Yang, H., Xu, X. (2022). Effects of water pollution on human health and disease heterogeneity: A review. *Frontiers in Environmental Science, 10*, 880246. https://doi.org/10.3389/fenvs.2022.880246

[11] Kulić Mandić, A., Bečelić-Tomin, M., Kerkez, Đ., Pucar Milidrag, G., Pešić, V., Prica, M. (2020). A mini review: Optimal dye removal by Fenton process catalysed with waste materials. In *Proceedings - The Tenth International Symposium GRID 2020* (pp. 205–211). https://doi.org/10.24867/grid-2020-p21

[12] Soufi, A., Hajjaoui, H., Elmoubarki, R., Abdennouri, M., Qourzal, S., Barka, N. (2021). Spinel ferrites nanoparticles: Synthesis methods and application in heterogeneous Fenton oxidation of organic pollutants – A review. *Applied Surface Science Advances, 6*, 100145. https://doi.org/10.1016/j.apsadv.2021.100145

[13] Valli Nachiyar, C., Rakshi, A. D., Sandhya, S., Britlin Deva Jebasta, N., Nellore, J. (2023). Developments in treatment technologies of dye-containing effluent: A review. *Case Studies in Chemical and Environmental Engineering, 7*, 100339. https://doi.org/10.1016/j.cscee.2023.100339

[14] Mehta, M., Sharma, M., Pathania, K., Jena, P. K., Bhushan, I. (2021b). Degradation of synthetic dyes using nanoparticles: A mini-review. *Environmental Science and Pollution Research, 28*(36), 49434–49446. https://doi.org/10.1007/s11356-021-15470-5

[15] Li, H., Wang, Y., Wang, Y., Wang, H., Sun, K., Lu, Z. (2019). Bacterial degradation of anthraquinone dyes. *Journal of Zhejiang University-SCIENCE B, 20*(6), 528–540. https://doi.org/10.1631/jzus.b1900165

[16] Khan, S., Noor, T., Iqbal, N., Yaqoob, L. (2024). Photocatalytic dye degradation from textile wastewater: A review. *ACS Omega, 9*(20), 21751–21767. https://doi.org/10.1021/acsomega.4c00887

[17] Yagub, M. T., Sen, T. K., Afroze, S., Ang, H. M. (2014). Dye and its removal from aqueous solution by adsorption: A review. *Advances in Colloid and Interface Science, 209*, 172–184. https://doi.org/10.1016/j.cis.2014.04.002

[18] Dutta, S., Bhattacharjee, J. (2022). A comparative study between physicochemical and biological methods for effective removal of textile dye from wastewater. In *Development in Wastewater Treatment Research and Processes* (pp. 1–21). https://doi.org/10.1016/b978-0-323-85657-7.00003-1

[19] Yadav, S., Tiwari, K. S., Gupta, C., Tiwari, M. K., Khan, A., Sonkar, S. P. (2023). A brief review on natural dyes, pigments: Recent advances and future perspectives. *Results in Chemistry, 5*, 100733. https://doi.org/10.1016/j.rechem.2022.100733

[20] Ardila-Leal, L. D., Poutou-Piñales, R. A., Pedroza-Rodríguez, A. M., Quevedo-Hidalgo, B. E. (2021). A brief history of colour, the environmental impact of synthetic dyes and removal by using laccases. *Molecules, 26*(13), 3813. https://doi.org/10.3390/molecules26133813

[21] Al-Tohamy, R., Ali, S. S., Li, F., Okasha, K. M., Mahmoud, Y. A.-G., Elsamahy, T., Jiao, H., Fu, Y., Sun, J. (2022). A critical review on the treatment of dye-containing wastewater: Ecotoxicological and health concerns of textile dyes and possible remediation approaches for environmental safety. *Ecotoxicology and Environmental Safety, 231*, 113160. https://doi.org/10.1016/j.ecoenv.2021.113160

[22] Chen, C.-X., Yang, S.-S., Pang, J.-W., He, L., Zang, Y.-N., Ding, L., Ren, N.-Q., Ding, J. (2024). Anthraquinones-based photocatalysis: A comprehensive review. *Environmental Science and Ecotechnology, 22*, 100449. https://doi.org/10.1016/j.ese.2024.100449

[23] Dulo, B., Phan, K., Githaiga, J., Raes, K., De Meester, S. (2021). Natural quinone dyes: A review on structure, extraction techniques, analysis and application potential. *Waste and Biomass Valorization*. https://doi.org/10.1007/s12649-021-01443-9

[24] Periyasamy, A. P. (2024). Recent advances in the remediation of textile-dye-containing wastewater: Prioritizing human health and sustainable wastewater treatment. *Sustainability, 16*(2), 495. https://doi.org/10.3390/su16020495

[25] Moyo, S., Makhanya, B. P., Zwane, P. E. (2022). Use of bacterial isolates in the treatment of textile dye wastewater: A review. *Heliyon*, *8*(6), e09632. https://doi.org/10.1016/j.heliyon.2022.e09632

[26] Oladoye, P. O., Ajiboye, T. O., Wanyonyi, W. C., Omotola, E. O., Oladipo, M. E. (2023). Ozonation, electrochemical, and biological methods for the remediation of malachite green dye wastewaters: A mini review. *Sustainable Chemistry for the Environment, 3*, 100033. https://doi.org/10.1016/j.scenv.2023.100033

[27] Masoud Ebratkhahan, H., S. N., Mahmoud Zarei, Abbas Jafarizad., Rostamizadeh, M. (2021). Removal of Neutral Red dye via electro-Fenton process: A response surface methodology modeling. *Electrocatalysis, 12*(5), 579–594. https://doi.org/10.1007/s12678-021-00640-3

[28] Mohammed, H. A., Khaleefa Ali, S. A., Basheer, M. I. (2020). Heavy metal ions removal using advanced oxidation (UV/H_2O_2) technique. *IOP Conference Series: Materials Science and Engineering, 870*, 012026. https://doi.org/10.1088/1757-899x/870/1/012026

[29] Soufi, A., Hajjaoui, H., Boumya, W., Elmouwahidi, A., Baillón-García, E., Abdennouri, M., Barka, N. (2024). Recent trends in magnetic spinel ferrites and their composites as heterogeneous Fenton-like catalysts: A review. *Journal of Environmental Management, 367*, 121971. https://doi.org/10.1016/j.jenvman.2024.121971

[30] Gayakwad, K., Ambade, B., Kumar, A., & Gautam, S. (2024). Sustainable solutions: Reviewing the future of textile dye contaminant removal with emerging biological treatments. *Limnological Review, 24*(2), 126–149. https://doi.org/10.3390/limnolrev24020007

[31] Slama, H. B., Chenari Bouket, A., Pourhassan, Z., Alenezi, F. N., Silini, A., Cherif-Silini, H., Oszako, T., Luptakova, L., Golińska, P., Belbahri, L. (2021). Diversity of synthetic dyes from textile industries, discharge impacts and treatment methods. *Applied Sciences, 11*(14), 6255. https://doi.org/10.3390/app11146255

[32] Periyasamy, A. P. (2024). Recent advances in the remediation of textile-dye-containing wastewater: Prioritizing human health and sustainable wastewater treatment. *Sustainability, 16*(2), 495. https://doi.org/10.3390/su16020495

[33] Hussain, S., Aneggi, E., Goi, D. (2021). Catalytic activity of metals in heterogeneous Fenton-like oxidation of wastewater contaminants: A review. *Environmental Chemistry Letters, 19*(3), 2405–2424. https://doi.org/10.1007/s10311-021-01185-z

[34] Lama, G., Meijide, J., Sanromán, A., Pazos, M. (2022). Heterogeneous advanced oxidation processes: Current approaches for wastewater treatment. *Catalysts, 12*(3), 344. https://doi.org/10.3390/catal12030344

[35] Cahyana, A. H., Liandi, A. R., Yulizar, Y., Romdoni, Y., Wendari, T. P. (2021). Green synthesis of $CuFe_2O_4$ nanoparticles mediated by *Morus alba* L. leaf extract: Crystal structure, grain morphology, particle size, magnetic and catalytic properties in Mannich reaction. *Ceramics International, 47*(15), 21373–21380. https://doi.org/10.1016/j.ceramint.2021.04.146

[36] Hachem, K., Ansari, M. J., Saleh, R. O., Kzar, H. H., Al-Gazally, M. E., Altimari, U. S., Hussein, S. A., Mohammed, H. T., Hammid, A. T.,Kianfar, E. (2022). Methods of chemical synthesis in the synthesis of nanomaterial and nanoparticles by the chemical deposition method: A review. *BioNanoScience, 12*(3), 1032–1057. https://doi.org/10.1007/s12668-022-00996-w

[37] Yadav, A. (2024). A review on synthesis methods of materials science and nanotechnology. *Advanced Materials Letters, 15*(3). https://doi.org/10.5185/amlett.2024.031758

[38] Tatarchuk, T., Shyichuk, A., Sojka, Z., Gryboś, J., Naushad, M., Kotsyubynsky, V., Kowalska, M., Kwiatkowska-Marks, S., Danyliuk, N. (2021). Green synthesis, structure, cations distribution and bonding characteristics of superparamagnetic cobalt-zinc ferrites

nanoparticles for Pb(II) adsorption and magnetic hyperthermia applications. *Journal of Molecular Liquids, 328*, 115375. https://doi.org/10.1016/j.molliq.2021.115375

[39] Naikoo, G. A., Mustaqeem, M., Hassan, I. U., Awan, T., Arshad, F., Salim, H., Qurashi, A. (2021). Bioinspired and green synthesis of nanoparticles from plant extracts with antiviral and antimicrobial properties: A critical review. *Journal of Saudi Chemical Society, 25*(9), 101304. https://doi.org/10.1016/j.jscs.2021.101304

[40] Pereira, L. M. S., Milan, T. M., Tapia-Blácido, D. R. (2021). Using response surface methodology (RSM) to optimize 2G bioethanol production: A review. *Biomass and Bioenergy, 151*, 106166. https://doi.org/10.1016/j.biombioe.2021.106166

[41] Szpisják-Gulyás, N., Al-Tayawi, A. N., Horváth, Z., László, Zs., Kertész, Sz., Hodúr, C. (2023). Methods for experimental design, central composite design and the Box–Behnken design, to optimise operational parameters: A review. *Acta Alimentaria, 52*(4), 521–537. https://doi.org/10.1556/066.2023.00235

[42] Veza, I., Spraggon, M., Rizwanul Fattah, I. M., Idris, M. (2023). Response surface methodology (RSM) for optimizing engine performance and emissions fueled with biofuel: Review of RSM for sustainability energy transition. *Results in Engineering, 18*, 101213. https://doi.org/10.1016/j.rineng.2023.101213

[43] Bayuo, J., Abukari, M. A., Pelig-Ba, K. B. (2020). Optimization using central composite design (CCD) of response surface methodology (RSM) for biosorption of hexavalent chromium from aqueous media. *Applied Water Science, 10*(6). https://doi.org/10.1007/s13201-020-01213-3

[44] Bhattacharya, S. (2021). Central composite design for response surface methodology and its application in pharmacy. In *IntechOpen eBooks*. https://doi.org/10.5772/intechopen.95835

[45] Lamidi, S., Olaleye, N., Bankole, Y., Obalola, A., Aribike, E., Adigun, I. (2022). Applications of response surface methodology (RSM) in product design, development, and process optimization. In *IntechOpen eBooks*. https://doi.org/10.5772/intechopen.106763

[46] Morshed, Pervez, Behary, Bouazizi, Guan, & Nierstrasz, 2023) doi: 10.1038/s41598-020-72401-z

[47] Rial, J. B., & Ferreira, M. L. (2021)) doi.org/10.1016/j.jwpe.2021.102065

[48] I.1.1 Jain, R., Mendiratta, S., Kumar, L., & Srivastava, A. (2021)) doi.org/10.1016/j.crgsc.2021.100086

[49] I.1.1 Bhaumik, M., Maity, A. & Brink, H.G. 2022). https://doi.org/10.1016/j.jcis.2021.11.181

[50] Shidiq, A. S., Permanasari, A., Hernani, Hendayana, S. (2021). The use of simple spectrophotometer in STEM education: A bibliometric analysis. *Moroccan Journal of Chemistry*, *9*(2), 290–300. https://doi.org/10.48317/IMIST.PRSM/morjchem-v9i2.27581

[51] González-Morales, D., Valencia, A., Díaz-Nuñez, A., Fuentes-Estrada, M., López-Santos, O., García-Beltrán, O. (2020). Development of a low-cost UV-Vis spectrophotometer and its application for the detection of mercuric ions assisted by chemosensors. *Sensors*, *20*(3), 906. https://doi.org/10.3390/s20030906

[52] Shi, Z., Chow, C. W. K., Fabris, R., Liu, J., Jin, B. (2022). Applications of online UV-Vis spectrophotometer for drinking water quality monitoring and process control: A review. *Sensors*, *22*(8), 2987. https://doi.org/10.3390/s22082987

[53] Slamani, S., Abdelmalek, F., Ghezzar, M. R., Addou, A. (2018). Initiation of Fenton process by plasma gliding arc discharge for the degradation of paracetamol in water. *Journal of Photochemistry and Photobiology A: Chemistry*, *353*, 140–148. https://doi.org/10.1016/j.jphotochem.2017.10.015

[54] Guo, C., Qin, X., Guo, R., Lv, Y., Li, M., Wang, Z., Li, T. (2021). Optimization of heterogeneous Fenton-like process with Cu-Fe@CTS as catalyst for degradation of organic matter in leachate concentrate and degradation mechanism research. *Waste Management*, *135*, 74–83. https://doi.org/10.1016/j.wasman.2021.08.021

[55] Mohadesi, M., Shokri, A. (2017). Evaluation of Fenton and photo-Fenton processes for the removal of p-chloronitrobenzene in aqueous environment using Box–Behnken design method. *Desalination and Water Treatment, 91*, 270–278. https://doi.org/10.5004/dwt.2017.21155

[56] Xu, H. Y., Liu, W. C., Qi, S. Y., Li, Y., Zhao, Y., Li, J. W. (2014). Kinetics and optimization of the decoloration of dyeing wastewater by a schorl-catalyzed Fenton-like reaction. *Journal of the Serbian Chemical Society, 79*(3), 361–377. https://doi.org/10.2298/JSC130225075X

[57] Xu, H. Y., Qi, S. Y., Li, Y., Zhao, Y. (2013). Heterogeneous Fenton-like discoloration of Rhodamine B using natural schorl as catalyst: Optimization by response surface methodology. *Environmental Science and Pollution Research, 20*(8), 5764–5772. https://doi.org/10.1007/s11356-013-1578-0

[58] Yang, C. W., Wang, D., Tang, Q. (2014). The synthesis of NdFeB magnetic activated carbon and its application in degradation of azo dye methyl orange by Fenton-like process. *Journal of the Taiwan Institute of Chemical Engineers, 45*(7), 2584–2589. https://doi.org/10.1016/j.jtice.2014.05.028.

[59] Lin, K.-Y. A., Hsu, F.-K. (2015). Magnetic iron/carbon nanorods derived from a metal organic framework as an efficient heterogeneous catalyst for the chemical oxidation process in water. *RSC Advances, 5*(63), 50790–50800. https://doi.org/10.1039/C5RA06043E

[60] en, D., Chen, S., Jiang, Y., Xie, S., Quan, H., Hua, L., Luo, X., Guo, L. (2017). Heterogeneous Fenton-like catalysis of Fe-MOF derived magnetic carbon nanocomposites for degradation of 4-nitrophenol. *RSC Advances, 7*(77), 49024–49030. https://doi.org/10.1039/C7RA09234B:contentReference[oaicite:5]{index=5}

[61] Li, W., Wu, X., Li, S., Tang, W., Chen, Y. (2018). Magnetic porous Fe_3O_4/carbon octahedra derived from iron-based metal-organic framework as heterogeneous Fenton-like catalyst. *Applied Surface Science, 436*, 252–262. https://doi.org/10.1016/j.apsusc.2017.11.151